Die approbierte Originalversion dieser Diplom-/Masterarbeit ist in der Hauptbibliothek der Technischen Universität Wien aufgestellt und zugänglich.
http://www.ub.tuwien.ac.at

The approved original version of this diploma or master thesis is available at the main library of the Vienna University of Technology.
http://www.ub.tuwien.ac.at/eng

Unterschrift des Betreuers

TECHNISCHE UNIVERSITÄT WIEN
Vienna University of Technology

D I P L O M A R B E I T

Sulfur poisoning of solid oxide fuel cells

Ausgeführt am Institut für

Chemische Technologien und Analytik

der Technische Universität Wien

unter Anleitung von Univ. Prof. Dr. Jürgen Fleig
und in Zusammenarbeit mit der AVL List GmbH, Dr. Gunther Weirum

durch

Jörg Mathé

Barmherzigengasse 19/11
1030 Wien

Ort, Datum

Unterschrift

Abstract

Fuel cells are a promising future technology for renewable energy sources. The electrochemical processes allow a highly efficient energy conversion. Due to the high operating temperatures of solid oxide fuel cells (SOFCs), they are also able to utilize carbon containing fuels. Therefore SOFCs can serve as an ideal companion at the transition from the use of fossil towards renewable energy sources. Sulfur compounds, as they are present in most fossil fuels, can have a highly negative impact on the catalytic processes in SOFCs even at low concentrations.

In the present work several parameters were varied, to investigate the influence of sulfur impurities in the fuel gas. The artificially mixed fuel simulated the output gas of a reformer, which is driven with diesel. A test rig using a furnace was successfully designed and built. Then measurements according to a test matrix were conducted in order to reveal the influence of changes in single parameters on SOFC operation. The standard parameters of the test matrix were: $c(H_2)$: 16.5 vol%, $c(H_2O)$: 10.7 vol%, $c(CO)$: 14.2 vol%, $c(CO_2)$: 10.1 vol%, $c(H_2S)$: 0.25 ppm, $c(SO_2)$: 0.29 ppm, c(hydrocarbon-mix): 738 ppm, $c(N_2)$: 48.4 vol%, I: 170 A/cm^2, fuel utilisation: 20.7 %, T: 735 °C.

The planned tests were carried out and the problems, which occured, could be solved. Amongst other things, it could be shown, that in the present tests hydrocarbons were still converted under the influence of sulfur poisoning.

Zusammenfassung

Brennstoffzellen sind eine vielversprechende Technologie für eine Zukunft mit erneuerbaren Energieträgern, da durch die elektrochemische Energieumwandlung sehr hohe Wirkungsgrade ermöglicht werden. Da Festoxid-Brennstoffzellen (SOFCs) bei hohen Temperaturen betrieben werden, sind sie in der Lage, auch kohlenstoffhaltige Brennstoffe umzusetzen. Daher sind sie ein idealer Wegbegleiter beim Übergang von der Nutzung fossiler Brennstoffe zu erneuerbaren Energiequellen. Schwefelverbindungen, wie sie in den meisten fossilen Brennstoffen vorkommen, können schon in kleinen Konzentrationen große Beeinträchtigungen der katalytischen Reaktionen innerhalb von SOFCs verursachen.

In dieser Arbeit wurde der Einfluss von Schwefelverunreinigungen im Brenngas unter Variation verschiedener Bedingungen untersucht. Das künstlich zusammengesetzte Brenngas simulierte das Produktgas eines Reformers, der mit Diesel betrieben wird. Nachdem ein Ofenprüfstand erfolgreich geplant und aufgebaut wurde, wurde ausgehend von Standardparametern Messungen gemäß einer Testmatrix durchgeführt, um den Einfluß von einzelnen Faktoren zu erkennen. Die Standardparameter waren: $c(H_2)$: 16.5 vol%, $c(H_2O)$: 10.7 vol%, $c(CO)$: 14.2 vol%, $c(CO_2)$: 10.1 vol%, $c(H_2S)$: 0.25 ppm, $c(SO_2)$: 0.29 ppm, c(Kohlenwasserstoff-Mix): 738 ppm, $c(N_2)$: 48.4 vol%, I: 170 A/cm^2, Brennstoffnutzung: 20.7 %, T: 735 °C.

Die geplanten Tests konnten durchgeführt und auftretende Probleme behoben werden. Es ließ sich unter anderem zeigen, dass Kohlenwasserstoffe unter dem Einfluss von Schwefelvergiftung im getesteten Gas noch umgesetzt wurden.

Contents

Acronyms **6**

1 Introduction **8**

2 Fuel cell basics **13**

2.1 Working principle of fuel cells 13

2.1.1 Cell voltage – Nernst-equation 15

2.1.2 Losses in fuel cell operation 16

2.1.3 Efficiencies 17

2.2 Fuel cell types and their characteristics 18

2.2.1 PEMFC — Polymer Electrolyte Membrane Fuel Cell (=PEFC) . 20

2.2.2 SOFC — Solid Oxide Fuel Cell 22

2.2.3 MCFC — Molten Carbonate Fuel Cell 23

2.2.4 PAFC — Phosphoric Acid Fuel Cell 23

2.2.5 AFC — Alkaline Fuel Cell 24

2.3 SOFC – designs and mechanisms 25

2.3.1 Cell designs 25

2.3.2 Materials 28

2.3.3 Fuel gases 32

2.3.4 SOFC cell voltage 33

3 Auxiliary power unit program at AVL **35**

4 Sulfur poisoning **38**

4.1 Impact on SOFC operation 40

4.2 Impact on reforming reactions 42

5 Experimental design and assembling **43**
5.1 Test setup 43
5.1.1 Cell housing 43
5.1.2 Test stand 46
5.1.3 Humidification tests 48
5.2 Start-up tests and procedures 51
5.3 Test matrix 53

6 Results and discussion **56**
6.1 Reference tests and regeneration periods 56
6.2 Carbon monoxide and carbon dioxide variation 58
6.3 Hydrocarbon variation 60
6.4 Water vapour variation 62
6.5 Current variation 64
6.6 Temperature variation 64
6.7 Table of characteristic numbers of all tests 67

7 Conclusion and outlook **69**

References **71**

Acronyms

AFC	alkaline fuel cell
AFL	anode functional layer
APU	auxiliary power unit
ASC	anode supported cell
CFL	cathode functional layer
CGO	cerium gadolinium oxide = GDC
CHP	combined heat and power
CSC	cathode supported cell
CTE	coefficient of thermal expansion
DEFC	direct ethanol fuel cell
DFAFC	direct formid acid fuel cell
EIS	electrical impedance spectroscopy
ESC	electrolyte supported cell
FCV	fuel cell vehicle
GC	gas chromatograph
GDC	gadolinia-doped ceria = CGO
HC	hydrocarbon
LSCF	lanthanum strontium cobalt ferrite
LSM	lanthanum strontium manganite
MCFC	molten carbonate fuel cell
MEA	membrane electrode assembly
MSC	metal supported cell
OCV	open circuit voltage
PAFC	phosphoric acid fuel cell
PEFC	polymer electrolyte fuel cell = PEMFC
PEMFC	polymer electrolyte membrane fuel cell = PEFC
PFSA	perfluorocarbon-sulfonic acid ionomer
PTFE	polytetrafluorethylen, Teflon

S/C	steam to carbon ratio
SOEC	solid oxide electrolysis cell
SOFC	solid oxide fuel cell
SSZ	scandium stabilized zirconia
TPB	triple phase boundary
TZP	tetragonal zirconia polycrystal
UPS	uninterruptible power supply
YSZ	yttria-stabilized zirconia

1 Introduction

Fuel cells are devices which convert chemical energy directly into electrical energy. Electrical charge is transfered due to a controlled electrochemical reaction between a reducing agent (fuel gas) and an oxidizer (typically oxygen in air). The transfered electrons are lead through a load to do electrical work. The process going on in a fuel cell represents the reversed electrolysis operation.

Fuel cells offer some advantages over other devices generating electricity and therefore have the potential to form the basis of reasonable alternatives to conventional applications. Fuel cells are able to operate at high efficiencies and with environmentally clean processes. If hydrogen is used as a fuel, the only by-products are water and heat, allowing an immission free electricity supply.

$$2\,H_2 \quad + O_2 \quad \longrightarrow 2\,H_2O + \text{energy} \tag{1.1}$$

$$\text{hydrogen} + \text{oxygen} \longrightarrow \text{water} + (\text{electrical power} + \text{heat}) \tag{1.2}$$

Certainly, hydrogen has to be perceived as an energy carrier. It is not an available ressource in the form of H_2, but has to be produced, stored and delivered to the consumer — e.g. the fuel cell. Major hydrogen sources are fossil fuels (hydrocarbons C_xH_y) and water (H_2O). In any way the energy needed for hydrogen production is greater than the energy provided by hydrogen usage, but hydrogen is well suited as a energy storage fed by renewable energy sources.

The maximum thermodynamic efficiency $\eta_{\text{th,max}}$ of fuel cells is [1]

$$\eta_{\text{th,max}} = 1 - \frac{T\,\Delta S}{\Delta H} \quad , \tag{1.3}$$

where ΔH is the reaction enthalpy (a negative value for exothermic reactions), T is the absolute temperature and ΔS is the change in entropy (either a positive or negative value depending on the fuel cell reaction). Therefore theoretically an efficiency greater than 100% would be possible with heat taken from surroundings.

In figure 1.1 the maximum thermodynamic efficiencies of a hydrogen fuel cell ($\Delta S < 0$

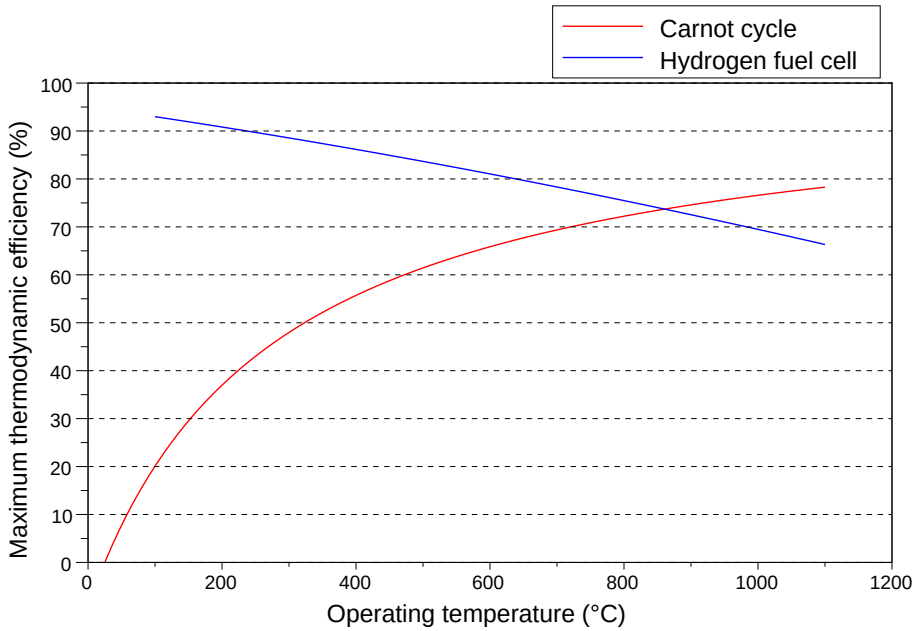

Figure 1.1: Maximum thermodynamic efficiencies of a heat engine (Carnot cycle, ambient temperature 25 °C) and a hydrogen fuel cell (product: water vapor), (thermodynamic data from [2])

and therefore $\eta_{\mathrm{th,max}} < 100\,\%$) and a heat engine is compared.

On the contrary conventional internal combustion engines (generally heat engines) are limited by the efficiency of a Carnot cycle, because the chemical energy is not directly converted into electricity, but firstly heat is generated which is then converted into kinetic energy and can subsequently be transformed into electrical power. The carnot efficiency $\eta_{\mathrm{th,carnot}}$ is

$$\eta_{\mathrm{th,carnot}} = 1 - \frac{T_{\mathrm{L}}}{T_{\mathrm{H}}} \tag{1.4}$$

where T_{L} and T_{H} are the temperatures of the low and the high heat reservoir which corresponds to the temperature of the surrounding (exhaust temperature) and the operating temperature.

Fuel cell applications can be categorized into portable, stationary and transport applications. Today fuel cells are already commercialized in a few sectors of the market, e.g combined heat and power (CHP) applications or as primary propulsion in forklifts and the like. The majority of fuel cell applications is still under development or on the step to market launch. Other fuel cell applications include uninterruptible power supplies (UPS), grid independent power generation, fuel cell electric vehicles, auxiliary power units (APUs) and portable products like battery chargers and personal electronics and

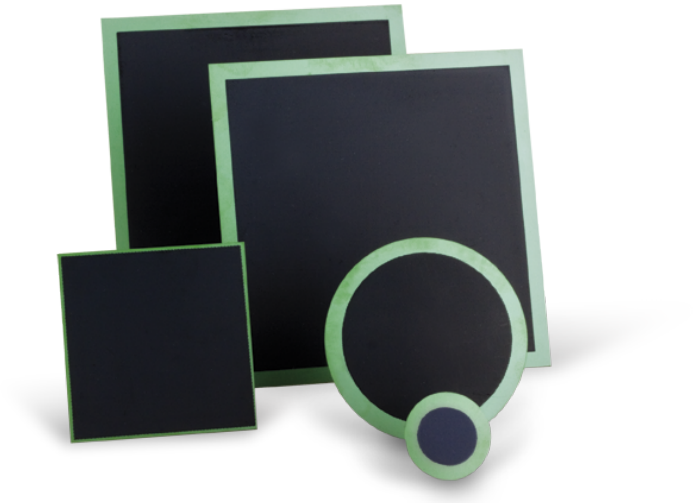

Figure 1.2: SOFC cells of the planar type by *AS Elcogen* [7]

educational kits [3, 4]. Each fuel cell application has its typical priorities in characteristics determined by the used fuel cell technology. Depending on the fuel cell type its strong points may be size, efficiency, emission, power density, simplicity, cost, durability, start-up time or robustness.

Despite the promising advantages, there are some difficulties and disadvantages of fuel cell technologies which have to be mastered. A big issue is degradation by various reasons like high load transients and fuel impurities, others are fuel accessibility, fuel production and fuel storage (in terms of power density). Research and Development is going on to work on this issues and show good results in many of these areas [5].

Fuel cells can possibly be powered by different kinds of fuels like hydrogen, methane, ethanol or even biomass using bacteria within the fuel cell [6]. Solid oxide fuel cells (SOFCs) and other high temperature fuel cells are able to use carbon containing fuels, such as natural gas, biogases or gasification gases or liquid hydrocarbons. This is not only a possibility for a use of other renewable resources but also a chance for fuel storages of higher energy density. A picture of some SOFCs is shown in figure 1.2. A brief description of all major fuel cell types is given in chapter 2.2 .

Along with the use of hydrocarbons comes an issue regarding sulfur. In many fuels sulfur compounds are either naturally contained or artificially added (e.g. odorant in natural gas for security reasons). In fuel cells catalysts are used to enable the fuel cell reactions and (where applicable) the internal reforming reactions. Those catalysts are

prone to blocking by sulfur — the so-called suphur poisoning.

Marine diesel fuel contains sulfur up to a level of 1 %, which is far too much for a fuel cell to operate. Even lower levels of about 10 ppm are damaging SOFC catalysts and levels of around 100 ppm could cause failure in about 1 hour of operation [8].

Besides sulfur (mostly in H_2S and SO_2 compounds in gaseous fuels and C−H−S compounds like tiophene in liquid fuels) there are other impurities in some fuel sources which can possibly cause problems. Among them are hydrochloric acid (HCl), chlorine (Cl_2), phosphine (PH_3), siloxane (R_2SiO, where R is a hydrogen atom or a hydrocarbon group) and many others. Those impurities are involved in different degradation mechanisms, with effects not only adding up in the presence of more than one compound but showing synergistic effects. [9–13]. Another relevant and connected problem is carbon deposition which leads to increased resistance by different effects [14].

The poisoning mechanisms of sulfur are not fully understood. Effects can be divided in an immediate and a long-term phase. Researchers generally agree on the short-term poisoning effect on solid oxide fuel cells, but long-term effects as well as characterisation of recovery processes, when sulfur free fuel is used after sulfur exposure, need to be further investigated [15].

The effect of sulfur poisoning is depending on many factors accounting for the fuel cell operating condition. An affected anode catalyst has impact on the entire fuel cell, hence often there is no clear cause-and-effect chain. Progress is made using electrical impedance spectroscopy (EIS) which to a certain degree allows to assign measured data to certain local effects within the fuel cell.

This study is part of a project at *AVL-List GmbH* developing an APU (see section 3) delivering electrical power to a truck during idle time. In the final system the SOFCs are fueled with diesel which is previously converted by a reformer.

The aim of this study is to investigate the response of SOFCs to a variation of various parameters connected with sulfur poisoning. SOFC single cell tests have been carried out to give a qualitative and quantitative characterization of the dependence of sulfur poisoning effects on the operating conditions. Parameters describing that conditions are e.g. temperature, fuel composition (varying concentrations of H_2, CO and CO_2, CH_4 and other hydrocarbons and H_2O) and the electrical load connected to the cell.

Sulfur poisoning of SOFCs is under investigation by several institutes and companies, resulting in a number of published studies. However in order to shorten testing time, in large part research groups investigated high sulfur concentrations. Due to the lack of detailed knowledge about reaction mechanisms only limited conclusions can be drawn

from those results of 'accelerated testing'. Furthermore many publications give information on sulfur poisoning in the absence of hydrocarbons (HCs) or on punctual cell states only. In order to fill this gap an experimental matrix within the desired parameter ranges is carried out within this work (see chapters 5 and to 6).

2 Fuel cell basics

2.1 Working principle of fuel cells

Fuel cells are able to generate electricity electrochemically directly out of external reactants. The reactants are the fuel gas at the anode, which is stored in an external reservoir, and an oxidizer at the cathode, where typically oxygen from the air is taken. So the reactants are supplied from the outside to the cell and the reaction products need to be removed. Hence fuel cells are able to be operated continuously and in a steady-state, unlike batteries where all reactants and products remain in the battery box (and therefore the energy is stored within the battery). Chemical energy is stored in the bonds of the reactants (fuel and oxidizer). Through an electrochemical reaction this energy is directly converted into electrical energy. Electrochemical reactions involve a changeover of electrons from one reactant to the other, where contrary to a normal combustion, the oxidation and the reduction reactions are spatially separated. As a result of this separation, electric current between the two electodes occurs in the form of electrons at the external circuit and ions (either positive or negative or both [16]) at the internal circuit. Without spatial separation of the oxidation and reduction reactions there would be no controlled flow of charge carriers, and therefore all chemical energy would be converted into expansion work and heat.

A typical fuel cell consists of 3 main parts, the anode, the cathode and the electrolyte with the two electrodes connected to an external circuit. The electrodes are enabling the reactions by catalytic activity and providing transport to all reactants and products to and from the reaction sites. Hence electrodes are typically porous structures increasing the catalytic surface and allowing fuel flow to shorten the paths, where ions need to be conducted. The electrolyte separates the two electrodes. It has to be electron insulating and ion conducting (the type of ion conductance depending on the fuel cell type).

There are several different fuels which can be used in fuel cells. In this chapter the working principle is explained using a hydrogen powered fuel cell with an oxide ion conducting electrolyte as example (as it is the case in a standard SOFC). Hydrogen is

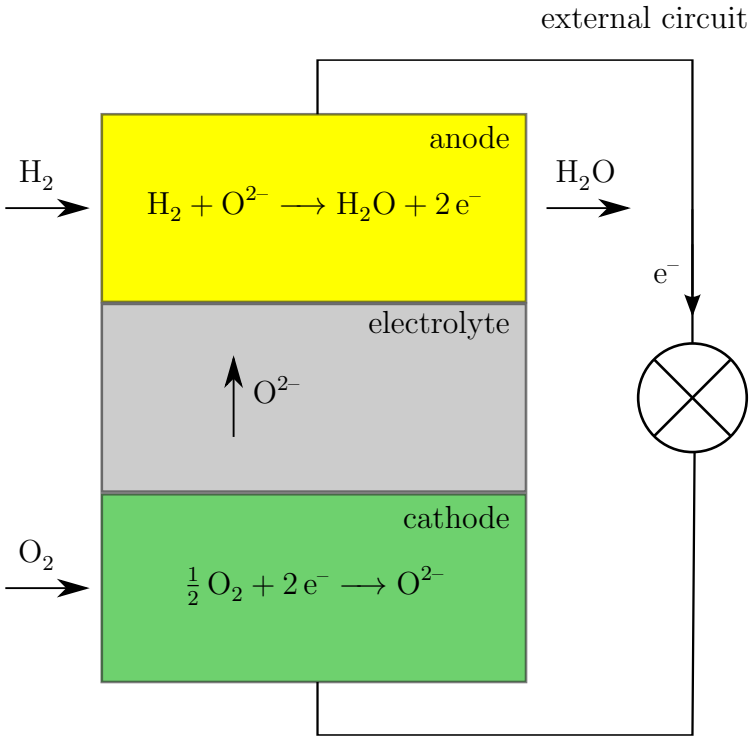

Figure 2.1: Principle of a fuel cell based on a oxygen ion conducting electrolyte fueled with hydrogen and oxygen

supplied to the anode and oxygen (air) to the cathode. By definition the anode is the electrode where the oxidation reaction occurs (loss of e^-) and the cathode is where the reduction reaction occurs (gain of e^-). Figure 2.1 illustrates the flow of reactants and products. They reach the electrolyte by diffusion through the porous electrode and react at the so-called triple phase boundary (TPB), where electrode (electron conducting), electrolyte (ion conducting) and fuel resp. oxidizer meet.

Those reactions at the electrodes are very unlikely to take place in a single step, but a number of elementary mechanisms, which cannot be clearly explained in all cases and are subject to research [17], add up to these reactions. Hence the terms global electrode reactions and overall fuel cell reaction are used. Those reactions for a oxygen ion conducting electrolyte are shown below.

global anode reaction	$H_2 + O^{2-} \longrightarrow H_2O + 2\,e^-$	(2.1)
global cathode reaction	$\frac{1}{2}\,O_2 + 2\,e^- \longrightarrow O^{2-}$	(2.2)
overall cell reaction	$H_2 + \frac{1}{2}\,O_2 \longrightarrow H_2O$	(2.3)

2.1.1 Cell voltage – Nernst-equation

The overall chemical reaction in a fuel cell has to be exothermic. A criterion of the direction of an chemical reaction is the Gibbs energy G (also called free enthalpy G), which is minimized in a spontaneous reaction, so

$$\Delta_{\mathrm{R}}G < 0 \qquad \text{for } T, p = \text{const} \tag{2.4}$$

with

$$\Delta_{\mathrm{R}}G = \sum_{\text{products}} G_{\mathrm{j}} - \sum_{\text{reactants}} G_{\mathrm{i}} \tag{2.5}$$

and

$$\Delta_{\mathrm{R}}G = \Delta_{\mathrm{R}}H - T\,\Delta_{\mathrm{R}}S \quad . \tag{2.6}$$

Theoretically $|\Delta_{\mathrm{R}}G|$ can be totally transformed into electrical energy

$$W_{\mathrm{el}} = -\Delta_{\mathrm{R}}G \tag{2.7}$$

$$= QU_{\mathrm{Nernst}} \tag{2.8}$$

which gives a maximum theoretical cell voltage U_C in operation of

$$U_{\mathrm{Nernst}} = \frac{-\Delta_{\mathrm{R}}G}{nF} \tag{2.9}$$

where $Q = nF$ is the transfered charge, $F = eN_{\mathrm{A}}$ is the Faraday constant and n is the number of electrons transfered in the considered global reactions. In the case of a fuel cell using pure hydrogen as fuel (see eqations 2.1ff) n equals 2 and $\Delta_{\mathrm{R}}G^0 = -237.2\,\mathrm{kJ/mol}$ at standard conditions (25 °C, 1 bar, the product will be liquid water), which gives $U_C^0 = 1.229\,\mathrm{V}$.

On the cathode there is a high oxygen concentration, while at the anode oxygen ions are instantly reacting with hydrogen to water (in the form of water vapour at SOFC operating conditions). This leads to a gradient in the chemical potential μ of oxygen between the two electrodes. Hence oxygen ions are moving from the anode to the cathode. If the external circuit is open, an electric field is produced until the gradient of the electrochemical potential $\tilde{\mu}$ of oxygen ions approaches zero and an equilibrium in

the electrolyte is established.

$$\tilde{\mu} = \mu + ze\varphi \tag{2.10}$$

$$\mu = \mu^0 + kT \ln a \tag{2.11}$$

where z is the charge number, e is the elementary charge and φ is the electrostatic potential and a is the activity of the species.

Using the equations above a term for the expected cell voltage depending on pressure and concentration, the Nernst equation can be derived. For any electrochemical reaction

$$\nu_1 A_1 + \nu_2 A_2 + \ldots \longrightarrow \ldots + \nu_{k-1} A_{k-1} + \nu_k A_k \tag{2.12}$$

the Nernst equation is

$$U_{\text{Nernst}} = -\frac{\Delta_{\text{R}} G^0}{nF} - \frac{RT}{nF} \ln \prod_{i=1}^{k} (a_i)^{\nu_i} \tag{2.13}$$

where the $|\nu_i|$ are the stoichiometric coefficients of the balanced reaction and are taken into account negatively for the educt side. Under the assumption of ideal gases the activities correspond to partial pressures, e.g. $a_{\text{H}_2} = p_{\text{H}_2} = P_{\text{H}_2}/P_0$. The Nernst equation for the hydrogen fuel cell can then be written as

$$U_{\text{Nernst}} = U^0_{\text{Nernst}} - \frac{RT}{nF} \ln \frac{p_{\text{H}_2\text{O}}}{p_{\text{H}_2} \sqrt{p_{\text{O}_2}}} \tag{2.14}$$

In literature the term electromotive force (EMF) is often used for the fuel cell voltage.

2.1.2 Losses in fuel cell operation

Losses caused by various effects are responsible for the deviation from the ideal cell voltage. Each loss is characteristic for a certain region of the voltage-current curve (I-V-curve, figure 2.2), even though all losses contribute in all areas.

The activation polarization (or activation voltage loss) is dominating in the region of low currents. It is caused by the energy barrier which has to be overcome for the electrochemical reactions to take place. Hence activation polarization occurs on both electrodes. Amongst others it is strongly impacted by temperature and the catalyst material and its condition including poisoning effects by impurities. In SOFC operation activation polarization at the anode is relatively low due to the high temperature [18],

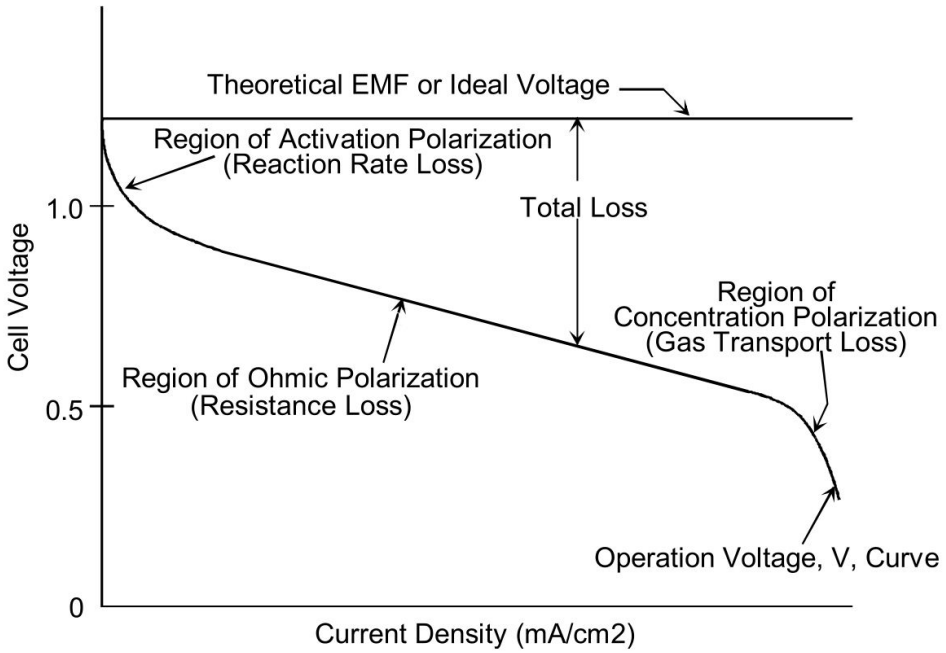

Figure 2.2: Losses in fuel cell operation related to its characteristic regions [20]

but possible sulfur compounds in the fuel stream are blocking reaction sites at the catalyst surface and can have great impact even at ppm levels [19].

The second region is caused by internal ohmic losses in the fuel cell. Contributing effects are the resistances for ionic and electronic conductance in the electrolyte resp. the electrodes and other parts conducting the electrons.

In the region of concentration polarization the supply of reactants is not sufficient for the high currents any more. Due to limitations in diffusion the concentration of reactants is decreased while the one of the products is increased. Hence the cell coltage is further decreased. In low temperature fuel cells the transport of liquid substances has to be considered [19].

2.1.3 Efficiencies

The total electric efficieny η_{el} of a fuel cell is defined as

$$\eta_{\mathrm{el}} = \frac{P_{\mathrm{el}}}{\Delta_{\mathrm{R}} H * \dot{n}_{\mathrm{fuel}}} \quad , \tag{2.15}$$

where P_{el} is the available electrical power output, $\Delta_{\mathrm{R}} H$ is the reaction enthalpy per mol fuel and $\dot{n}_{\mathrm{fuel}}$ is the molar flow rate of supplied fuel. The total electrical efficiency can

be decomposed to a product of efficiencies of different types [21].

The maximum thermodynamic efficiency $\eta_{\mathrm{th,max}}$ is linked to the Nernst-equation.

$$\eta_{\mathrm{th,max}} = 1 - \frac{T\,\Delta S}{\Delta_{\mathrm{R}} H} = \frac{\Delta_{\mathrm{R}} G}{\Delta_{\mathrm{R}} H} \tag{2.16}$$

$$\text{with} \qquad \Delta_{\mathrm{R}} G = \Delta_{\mathrm{R}} G^0 + RT \ln \frac{\prod_{\mathrm{products}} (a_i)^{\nu_i}}{\prod_{\mathrm{reactants}} (a_j)^{\nu_j}} \tag{2.17}$$

It depends on temperature, pressure and fuel composition. An increased temperature has a negative effect on $\eta_{\mathrm{th,max}}$ for hydrogen and carbon monoxide due to the entropy change, while there is only a negligible effect when using methan and a possible positive effect for other fuels. Pressure and fuel concentration effects are reflected in the activities (see also section 2.1.1).

The voltage efficiency

$$\eta_V = \frac{U_{\mathrm{cell}}}{U_{\mathrm{Nernst}}} \tag{2.18}$$

with the actual non-equilibrium cell voltage U_{cell} covers all losses which occur during fuel cell operation discussed in section 2.1.2.

The fuel utilisation η_{fu} takes the actually used amount of fuel into account.

$$\eta_{\mathrm{fu}} = \frac{\text{rate of fuel converted}}{\text{rate of fuel supplied}} \tag{2.19}$$

At a high η_{fu} the oxygen partial pressure at the anode increases, which may cause oxidation at the anode. Therefore fuel utilisations of less than 85 % are common [21].

The total electrical efficiency can now be written as

$$\eta_{\mathrm{el}} = \eta_{\mathrm{th,max}} * \eta_{\mathrm{fu}} * \eta_V \quad . \tag{2.20}$$

2.2 Fuel cell types and their characteristics

Different types of fuel cells are conventionally classified by their electrolyte material. Figure 2.3 gives an overview of all major fuel cell types showing involved reactants and temperature ranges.

Furthermore fuel cells can be categorized in low temperature fuel cells working in a range from ambient temperature to about 250 °C and high temperature fuel cells operating at above 600 °C. Today there are no competitive fuel cells in the intermediate range, though benefits would be a higher heat quality than in the lower and less material

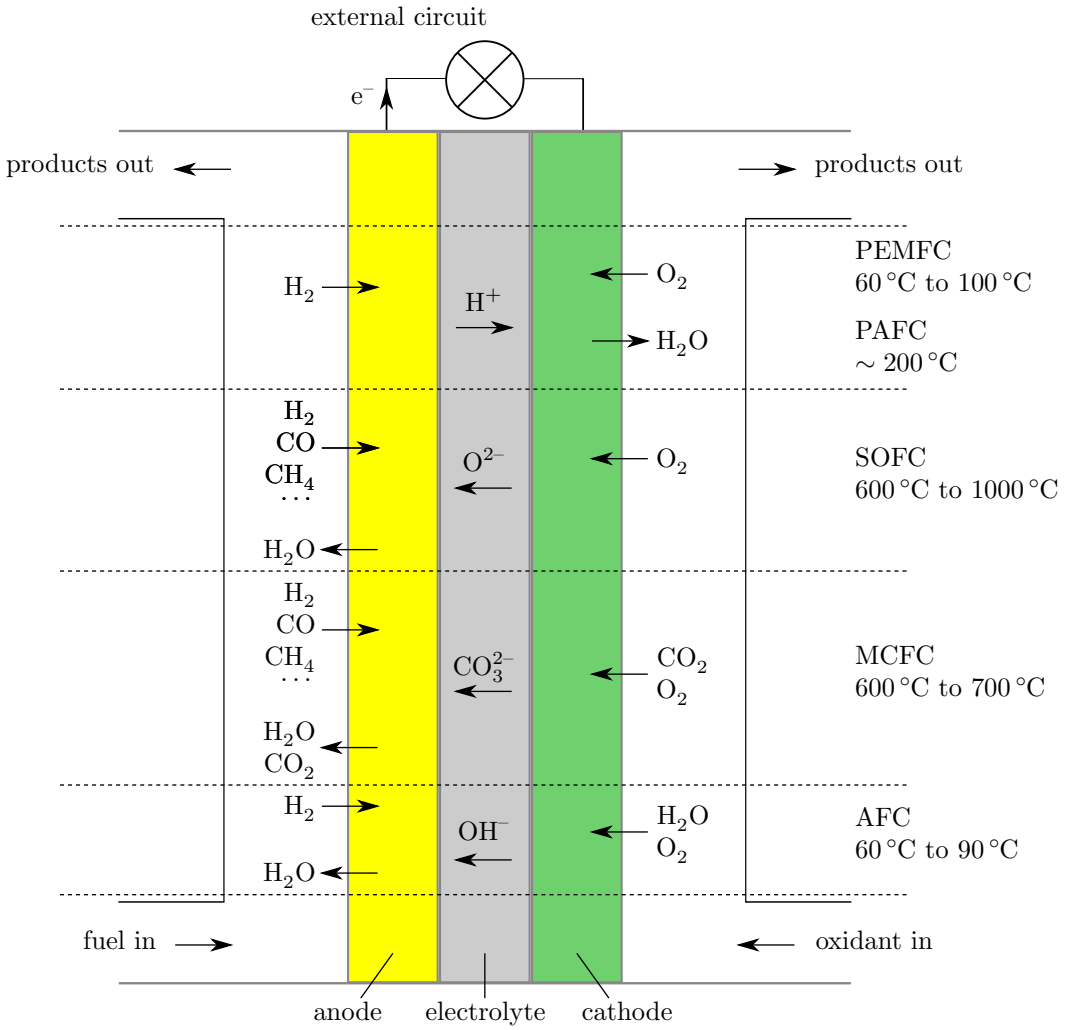

Figure 2.3: Overview of flows of reactants and temperatures of major fuel cell types

durability issues than in the higher temperature range.

On the one hand a lower working temperature offers a shorter start-up time and higher efficiency, but on the other hand more expensive noble metal catalysts are required. Besides a higher heat quality the major advantage of fuel cells working in the high temperature range is fuel flexibility.

While cells fueled with pure hydrogen have water (liquid or gaseous) as exhaust gas only, other fuels can cause emissions containing CO_2, CO or unused fuel.

The APU developed at *AVL* runs on diesel (see section 3). Therefore a catalytic converter is used to ensure a complete combustion in the APU.

2.2.1 PEMFC — Polymer Electrolyte Membrane Fuel Cell (=PEFC)

The PEMFC or PEFC (Polymer Electrolyte Fuel Cell) — also named proton exchange membrane fuel cell — is best known of all fuel cell types, because of its applications especially in fuel cell vehicles (FCV), but also in a variety of other fields. In PEMFCs hydrogen ions (protons) are passing the electrolyte as seen in the following equations characterizing the reactions at the electrodes.

$$\text{anode:} \qquad \mathrm{H_2} \longrightarrow 2\,\mathrm{H^+} + 2\,\mathrm{e^-} \tag{2.21}$$

$$\text{cathode:} \quad \tfrac{1}{2}\,\mathrm{O_2} + 2\,\mathrm{H^+} + 2\,\mathrm{e^-} \longrightarrow \mathrm{H_2O\,(l)} \tag{2.22}$$

The essential part of a PEM fuel cell is its PTFE- (Teflon)-like polymer membrane featuring some important characteristics. It is impermeable to gases and non-conducting electrons, but conducting protons. The thin membrane (thickness in the order of 0.1 mm) is located between the two porous electrodes. As the working temperature of PEMFCs is typically in the range of 60 °C to 100 °C, nobel metals as catalysts are needed. Both electrodes are usually made of platinum as a catalyst on a porous carbon support. The assembly of those layers is refered to as the membrane electrode assembly (MEA). Electrical efficiencies of 40 % to 50 % can be achieved [22].

The main advantages of PEM fuel cells are linked to its relatively low temperature. There is a possibility of a quick start-up, little stresses on materials occur and sealing of the cells can be achieved quite easily.

The best-known membrane material, Nafion® made by *Dupont*, which is in use over decades, and other similar materials are made out of perfluorocarbon-sulfonic acid ionomer (PFSA) [23]. Modifications of PFSA membranes and completely new polymers are under recent investigation [24]. The PSFA structure has a hydrophobic backbone based on PTFE and a highly hydrophilic side chain ending with group of a SO_3^- with an ionic bond to a H^+ ion. Movement of the H^+ ions is possible when the membrane is well hydrated (up to 50 % by weight) [23]. Hence to enable proton conductivity there has to be a sufficient content of water in the fuel gas stream and the temperature must not exceed the boiling point of water at operating pressure.

PEMFC fuel has to be free from carbon monoxide (and has to be externally cleaned if produced out of carbon containing fuels), because CO poisons the active platinum sites even at concentrations of around 10 ppm [24]. Operation at higher temperatures would improve reaction kinetics and therefore diminish this problems, but would cause

problems with the PFSA membranes. While operating below the boiling point of water, one has to consider the removal of the liquid H_2O product molecules in order not to block the catalyst sites at cathode.

DMFC — Direct Methanol Fuel Cell

In literature the direct methanol fuel cell is partly refered to as a fuel cell of another type, but according to the classification by electrolyte it should be considered as a subtype of the PEMFC. In a DMFC methanol (CH_3OH) is internally converted into carbon dioxide and hydrogen. Below are the global reactions occuring at the electrodes.

$$\text{anode:} \quad \mathrm{CH_3OH + H_2O \longrightarrow CO_2 + 6\,H^+ + 6\,e^-} \tag{2.23}$$

$$\text{cathode:} \quad \mathrm{\tfrac{3}{2}\,O_2 + 6\,H^+ + 6\,e^- \longrightarrow 3\,H_2O} \tag{2.24}$$

The DMFC uses methanol mixed with water either liquid or gaseous, depending on the electrolyte. The operating temperature range is 60 °C to 130 °C. Since the reaction in 2.23 is relatively slow, DMFCs themselves have a low power density [25], although the energy density of liquid methanol is higher than that of hydrogen (compressed to 300 bar) [26]. The internal reforming of methanol is taking place in several steps with intermediates as CO which blocks catalyst sites (therefore a higher amount of platinum as catalyst is needed), which results in a lower efficiency than operation with pure hydrogen [24].

Improvement of the catalyst material (increasing reforming performance) is done by using platinum-ruthenium (Pt-Ru) or platinum-ruthenium-tin (Pt-Ru-Sn) mixtures [25]. A higher temperature would speed up kinetics with the drawback of increased methanol crossover. To a certain degree methanol is able to diffuse through the electrolyte resulting in a decreased voltage and a loss of fuel (those electrons do not pass the external circuit).

The main advantage of DMFCs is the liquid fuel which is easy to handle and offers a high energy density. A problem is the poisonousness of methanol, that is why storing of pure methanol is illegal in some countries [26]. DMFCs are applied mainly in portables and also in vehicles and off-grid applications, but due to their lower efficiency, not in power stations [27].

Other PEMFC subtypes

There are other subtypes of the PEM fuel cell of minor importance, e.g. the direct ethanol fuel cell (DEFC) or the direct formid acid fuel cell (DFAFC) which are aimed at

having better crossover characteristics, but usually have slower internal reforming [28].

2.2.2 SOFC — Solid Oxide Fuel Cell

The present experimental work is done using solid oxide fuel cells. This section is an overview for comparison with other fuel cell types. A more detailed description of SOFC materials, processes, design and operation is given in section 2.3.

SOFCs are working in a temperature range of 600 °C to 1000 °C. The electrolyte material is a solid, non-porous ceramic conducting oxide ions at this temperature, while it is insulating at lower temperatures. The standard materials are yttria-stabilized zirconia (YSZ, ZrO_2 doped with 8 to 10 mol% Y_2O_3) for SOFCs with a thin electrolyte layer, zirconia doped with less yttria, which offers better mechanical stability and scandium stabilized zirconia for use with a supporting electrolyte layer and cerium gadolinium oxide [26, 29]. The anode is commonly made out of a cermet of nickel and the electrolyte material and the standard materials for the cathode are lanthanum strontium manganite (LSM) and lanthanum strontium cobalt ferrite (LSCF). The overall reactions at the electrodes are below.

$$\text{anode:} \quad H_2 + O^{2-} \longrightarrow H_2O + 2\,e^- \tag{2.25}$$

$$\text{cathode:} \quad \tfrac{1}{2}\,O_2 + 2\,e^- \longrightarrow O^{2-} \tag{2.26}$$

Besides hydrogen, carbon monoxide can be directly used as fuel. Other fuels can be used with SOFCs due to internal reforming or maybe even directly [18]. When providing water within the fuel stream at SOFC operating temperatures the steam reforming reaction

$$CH_4 + H_2O \longrightarrow 3\,H_2 + CO \tag{2.27}$$

and the water gas shift reaction

$$CO + H_2O \longrightarrow H_2 + CO_2 \tag{2.28}$$

occur on the catalyst. An external reformer can be employed to enable operation with higher hydrocarbons as fuel. This opens up the possibility of usage of various fuel sources, which unfortunately partly contain impurities like sulfur (e.g. diesel). Attention has also be drawn to the water content in the fuel to avoid carbon deposition.

The APU by *AVL* takes advantage of this fuel versatility by using diesel, so no addi-

tional media have to be installed on-board of a truck.

Advantages of SOFCs over fuel cells of other types operating in the high temperature range are the absence of any liquid component and its associated issues.

2.2.3 MCFC — Molten Carbonate Fuel Cell

In MCFCs the electrolyte conductance is provided by carbonate ions (CO_3^{2-}) in a molten carbonate salt mixture (Li_2CO_3 and K_2CO_3 at atmospheric or Li_2CO_3 and Na_2CO_3 at elevated pressure systems [25]). For stability the electrolyte is suspended in a porous, chemically inert aluminate matrix (e.g. $LiAlO_2$). At the electrodes the following global reactions take place.

$$\text{anode:} \qquad H_2 + CO_3^{2-} \longrightarrow H_2O + CO_2 + 2\,e^- \tag{2.29}$$

$$\text{cathode:} \qquad \tfrac{1}{2}\,O_2 + CO_2 + 2\,e^- \longrightarrow CO_3^{2-} \tag{2.30}$$

The overall cell reaction is

$$H_2 + \tfrac{1}{2}\,O_2 + CO_2\,(\text{cathode}) \longrightarrow H_2O + CO_2\,(\text{anode}) \tag{2.31}$$

In most designs the carbon dioxide output from the anode is recycled as input to the cathode, so there is a need for an external fuel processing/CO_2 circulation loop [25]. MCFCs operate in a typical temperature range of 600 °C to 700 °C. Hence no noble metals are needed and typically nickel resp. nickel oxide is used as a catalyst at the anode and the cathode.

Due to the high operating temperature, internal reforming can take place at the anode allowing the use of other fuels than H_2 like CO and CH_4.

Since MCFCs allow slow start-ups only and because of the electrolyte/CO_2 handling, they are mainly used for medium and large power applications producing an output from 10 kWe up to MWs, where they are one of the key technologies [27, 28].

2.2.4 PAFC — Phosphoric Acid Fuel Cell

While historical PAFCs used down to 85% phosphoric acid (H_3PO_4) in water [20] nowadays pure H_3PO_4 is used as electrolyte. It is proton (H^+) conducting. The global

reaction equations at the electrodes of a PAFC are shown below.

$$\text{anode:} \qquad \mathrm{H_2} \longrightarrow 2\,\mathrm{H^+} + 2\,\mathrm{e^-} \tag{2.32}$$

$$\text{cathode:} \quad \tfrac{1}{2}\,\mathrm{O_2} + 2\,\mathrm{H^+} + 2\,\mathrm{e^-} \longrightarrow \mathrm{H_2O} \tag{2.33}$$

On both the anode and the cathode Pt is used as a catalyst, the electrodes itself being a carbon structure (carbon paper). The typical operating temperature of PAFCs is about 200 °C, which results in relatively high grade heat. A total efficiency of around 85 % can be achieved when utilizing the heat with an electric efficiency of 40 % to 50 % [22, 27]. PAFCs do not show any CO_2 poisoning effect and due to the elevated temperature a better CO tolerance than PEMFCs. The melting point of phosphoric acid is about 40 °C which has to be taken into account at start-up.

PAFCs are almost solely applied in the large stationary sector ($P > 200\,\mathrm{kWe}$) [27].

2.2.5 AFC — Alkaline Fuel Cell

Alkaline fuel cells usually operate on a water based potassium hydroxide (KOH) solution as electrolyte. This electrolyte is conducting hydroxil ions (OH^-) which allows the electrode reactions as below.

$$\text{anode:} \qquad \mathrm{H_2} + 2\,\mathrm{OH^-} \longrightarrow 2\,\mathrm{H_2O} + 2\,\mathrm{e^-} \tag{2.34}$$

$$\text{cathode:} \quad \tfrac{1}{2}\,\mathrm{O_2} + \mathrm{H_2O} + 2\,\mathrm{e^-} \longrightarrow 2\,\mathrm{OH^-} \tag{2.35}$$

At both electrodes nickel can be used as catalyst. Although some historically important alkaline fuel cells have operated at about 200 °C [30], the typical temperature range of AFCs is 60 °C to 90 °C. Low temperature cells are recently designed to operate down to 23 °C [22] [27]. Hence a relatively quick start-up of the cell is possible.

A major disadvantage of AFCs is the vulnerability to carbon dioxide poisoning of KOH. CO_2 is absorbed forming K_2CO_3, thereby reducing the OH^- concentration which leads to decreased ionic conductivity as well as increased electrolyte viscosity [31]. In order to prevent a decreased operation efficiency one may remove the CO_2 from the air or use a larger quanitity of (circulating) KOH. The substitution of KOH by e.g. sodium hydroxide (NaOH) would be possible, but NaOH shows much lower solubility of sodium carbonate compared to potassium carbonate [32].

AFCs are able to operate at a high electrical efficiency of up to 70% with a high power-density, but because of the CO_2 issue and the corrosiveness of the electrolyte,

AFCs have a very small impact on the fuel cell market. Due to its characteristics AFCs are used in space applications, where pure oxygen is available and one can benefit from the produced water [22].

2.3 SOFC – designs and mechanisms

2.3.1 Cell designs

In SOFCs all three main parts, the anode, the electrolyte and the cathode are solid at both standard and operating conditions. Various different SOFC designs exist, with the planar and tubular designs most widely used.

The planar design is relatively easy to manufacture and offers a higher power density (up to $2\,W/cm^2$ [33]). Its main difficulty is achieving a good sealing to prevent gas leakage or cross-leakage from one electrode to the other as well as electrical shorts and mechanical damage (high temperature change at startup and shutdown accompanied by a thermal expansion mismatch). Sealing is established by applying compressive loads or by using high temperature sealants or both [33]. In order to obtain minimal resistances and mechanical stability at the same time, different planar designs have been developed, where one layer is the mechanical support layer and the others are kept very thin (figure 2.4). Nowadays anode supported cells (ASC) and metal supported cells (MSC, an external layer is supporting) are the most promising designs. Typical dimensions for the electrolyte in electrolyte supported cells (ESC) are thicker than 100 µm, for non-ESC from less than 1 µm to 20 µm [33]. Cathode thicknesses of ESC, ASC and MSC SOFCs range from 20 µm to 100 µm. The size of the supporting layer in ASC and MSC cells is typically above 300 µm. Typical sizes of planar SOFCs reach from button size up to 20x20 cm.

The other important SOFC design is the tubular SOFC design (introduced by Westinghouse, now Siemens [34]) as shown in figure 2.5. Because of its layout there is no need for a high temperature sealing along the length of the tube, which is a big advantage. Tubular SOFCs have a lower power density than planar cells at around $0.3\,W/cm^2$. Power density is increased by decreasing the tube diameter from above 15 mm to far below 5 mm, so-called microtubular cells. A drawback of the tubular design is its more difficult manufacturing process [33].

In this work single cells of the planar type were used. The tested SOFCs by *Topsoe Fuel Cell A/S* were of the ASC type.

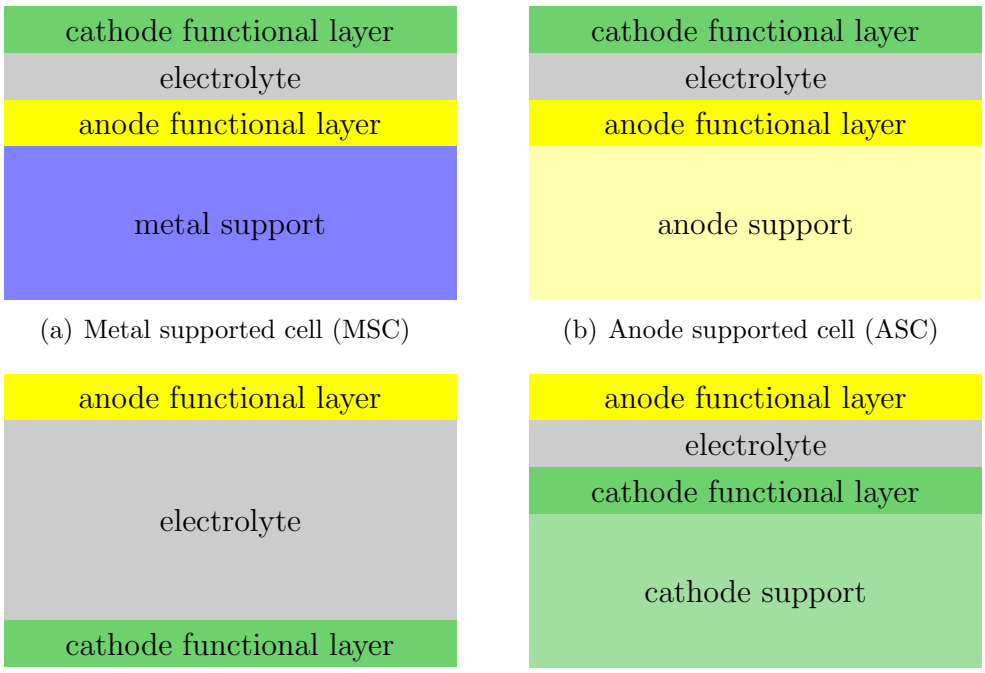

(a) Metal supported cell (MSC)

(b) Anode supported cell (ASC)

(c) Electrolyte supported cell (ESC)

(d) Cathode supported cell (CSC)

Figure 2.4: Schematic of planar SOFC support designs (not drawn to scale), for typical thicknesses see text.

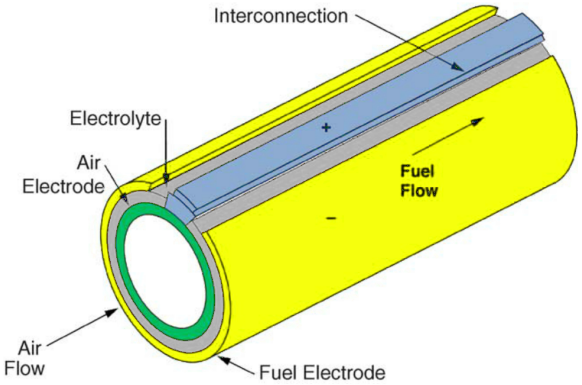

Figure 2.5: Sealless tubular SOFC design by Westinghouse, now Siemens [35]

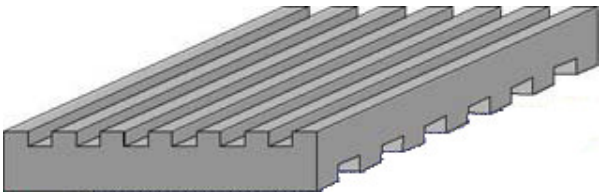

Figure 2.6: Drawing of an interconnector with flow channels featuring cross flow for use in SOFC stacks with planar cells

A single SOFC does not provide a lot of energy, hence for many applications several cells are integrated into a stack. Planar cells are stacked together and connected in series, while tubular cells depending on their size often have a mixed series and parallel configuration. This is an advantage in the case of failure of a single tube, because current is distributed on the parallel ones.

Other components necessary for SOFC operation are current collectors and a gas supply to the cell, which are combined with each other in many cell designs. Current collectors conduct electrons from the anode to the external circuit and on the other side from the external circuit to the cathode. In a planar SOFC stack interconnectors provide a path for electrons from the anode of one cell to the cathode of the adjacent cell and also serve as gas supply of the cells via gas flow channels, as shown in figure 2.6. At both anode and cathode the gas composition changes while flowing along a planar cell. Therefore to optimize the gas supply different modes of gas flow through the channels are used. Perpendicular gas flow (cross-flow) makes the gas supply easy to handle, but leads to less fuel utilisation and a diagonal temperature distribution. Gas flow of opposed orientations (counter-flow) yield a better fuel utilisation and a comparatively even temperature distribution. Flow of the same direction (co-flow) requires a challenging way of gas supply and shows a strongly non-uniform temperature and load distribution, but leads to the highest fuel utilisation. The electrical connection between current collectors and electrodes is improved by metal meshes (e.g. out of nickel or platinum) and possible cathode paste and nickel foam which are all pressed together. Layers improving the electrical contact can also be applied into the electrodes themselves to reduce the number of components [26, 33].

2.3.2 Materials

Electrolyte

A material used as a SOFC electrolyte has to fulfill a number of requirements. It has to offer a good ionic and low electronic conductivity. It has to be dense and leak-tight also when used as a thin layer. It has to be chemically stable at operating and room temperatures and under both oxidizing und reducing conditions. It should cope with thermal stresses and be of low cost. Nowadays the material of choice for planar ASC cells is yttria-stabilized zirconia (YSZ), which is widely used since the 1970s in oxygen sensors e.g. in automobile exhausts. Research is carried out on other suitable materials especially for operation at lower temperature [36]. YSZ is utilized in the cells by *Topsoe Fuel Cell A/S* under investigation in the current work.

Pure zicronia (ZrO_2) is undergoing phase transitions from cubic to tetragonal to monoclinic phases from high to low temperatures. By doping with cations like Ca^{2+}, Y^{3+} or Sc^{3+} (compared to Zr^{4+}) the cubic phase can be maintained down to room temperature [29]. Usually a doping concentration of 8 mol% Y_2O_3 is used for SOFCs (denominated 8YSZ). For a better long term stability 10YSZ may be a better choice and ZrO_2 doped with 3 mol% of Y_2O_3 (called TZP, tetragonal zirconia polycrystal) possesses better mechanical strength at room temperature [37].

The doping of Y_2O_3 into ZrO_2 leads to formation of vacant oxygen sites which can be written in Kröger–Vink notation [38]

$$Y_2O_3(ZrO_2) \longrightarrow 2\,Y'_{Zr} + 3\,O_O^{\times} + V_O^{\bullet\bullet} \tag{2.36}$$

This structure strongly improves oxygen ion conductivity σ_O

$$\sigma_O = 2F[V_O^{\bullet\bullet}]u_O \tag{2.37}$$

with its mobility u_O, and the molar concentration of vacancies in oxygen sites $[V_O^{\bullet\bullet}]$. At a level of about 8 mol% $[V_O^{\bullet\bullet}]$ the conductivity reaches a maximum due to local ordering of the vacancies at a higher $[V_O^{\bullet\bullet}]$. Though using Sc_2O_3 as dopant would give a better conductivity, it is not prefered because of material cost [37]. Figure 2.7 shows the ionic conductivity depending on dopant and temperature.

Allowing a loss of 100 mV gives a maximum electrolyte thickness of about 100 µm at 1000 °C, which is usable for ESC type of cells (see figure 2.4). Due to fragility ESC cells are not feasible with YSZ as electrolyte at lower temperatures.

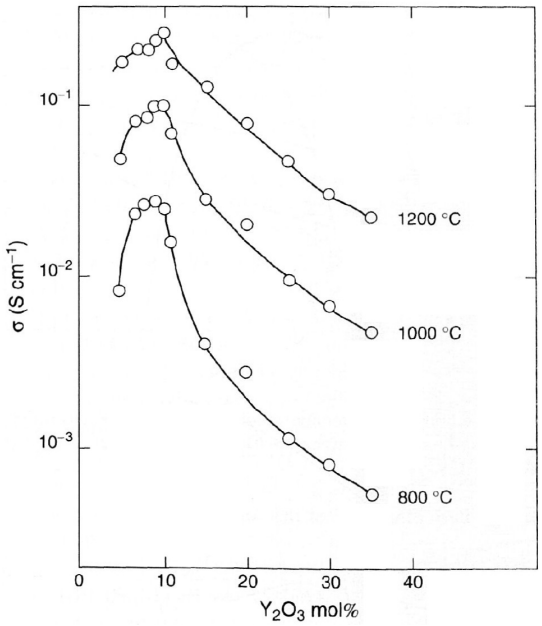

(a) Dependence on dopant concentration

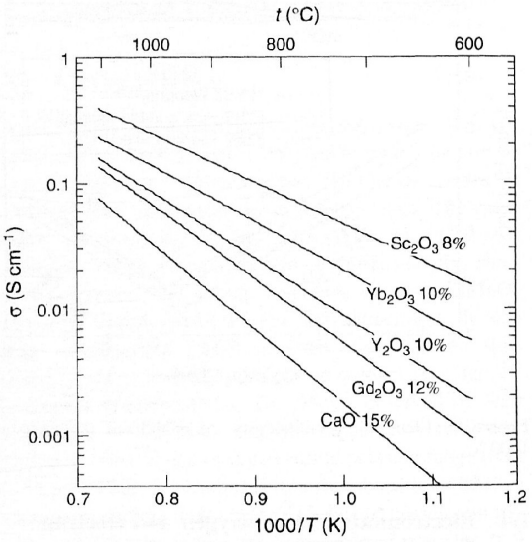

(b) Dependence on temperature and dopant species

Figure 2.7: Ionic conductivity of doped ZrO_2 [37, 39–41]

Like all other solid oxides, YSZ shows a non-zero electronic conductivity, strongly depending on the concentration of charge carriers (holes and electrons), which are generated in the oxidation or reduction reactions [37]

$$\mathrm{O_O} \longrightarrow \mathrm{V_O^{\bullet\bullet}} + 2\,\mathrm{e} + \tfrac{1}{2}\,\mathrm{O_2}\ , \qquad K_1 = \frac{[\mathrm{V_O^{\bullet\bullet}}]n^2 P_{\mathrm{O_2}}^{1/2}}{[\mathrm{O_O}]} \tag{2.38}$$

$$\mathrm{V_O^{\bullet\bullet}} + \tfrac{1}{2}\,\mathrm{O_2} \longrightarrow \mathrm{O_O} + 2\,\mathrm{h}\ , \qquad K_2 = \frac{[\mathrm{O_O}]p^2}{[\mathrm{V_O^{\bullet\bullet}}]P_{\mathrm{O_2}}^{1/2}} \tag{2.39}$$

with the concentration of electrons n and of holes p.

Typical oxygen partial pressures of SOFC operating conditions are in the range of 10^{-20} atm to 0.21 atm and only at pressures of about 10^{-30} atm the electronic conductivity may become comparable to the ionic conductivity [36].

The optimum thickness of an YSZ electrolyte with respect to ohmic loss and oxygen permeation through the electrolyte at 1000 °C is around 100 µm for 0.1 A/cm^2 and 10 µm for 1 A/cm^2 [37].

Anode

A lot of demands are made on the SOFC anode material, which is porous allowing gas diffusion to the reaction sites. It has to offer a catalytic activity for the electrochemical SOFC reactions as well as for fuel processing, preferably not showing hydrocarbon pyrolysis with carbon deposition. The anode material has to conduct electrons and an ionic conductivity is preferable in order to expand the electrochemically active surface to the full spatial anode region (see figure 2.8). For these properties to be contained it needs a stable microstructure. Furthermore, the anode has to be chemically stable when getting in contact with the electrolyte, current collectors, fuel and ideally even air from room to operating temperature. The material should have a matching thermal expansion coefficient (CTE) to the electrolyte to minimize mechanical stresses at startup and shutdown. [37, 42]

Nickel has proofed itself as a catalytic material in steam reformation, but is not stable at high temperatures and has a big CTE mismatch compared to YSZ (Ni: 16×10^{-6}, 8YSZ: 10×10^{-6}) [37]. In order to adapt the properties a Ni-YSZ cermet (a compound of **cer**amic and **met**al) is used. For CTE fitting and ionic conductivity a low Ni to YSZ ratio would be prefered. The electronic conductivity of a Ni-YSZ cermet rises abruptly at about 30 % Ni [37].

In cells of the ASC type the anode is furthermore required to support the whole cell mechanically. Those thicker anodes are preferably inhomogeneous. In order to maximize the TPB a higher nickel amount and finer microstructure is applied in the so-called anode functional layer (AFL) close to the electrolyte. Due to limitations in ion conductivity the more distant part serves mostly for electron conductivity, gas transport and mechanical support [26].

Unfortunately nickel is very prone to deactivation by sulfur. A material showing more sulfur tolerance is found in combination of nickel with Sc_2O_3-doped ZrO_2 (SSZ). Ni-SSZ anodes and/or SSZ electrolytes show better results in sulfur poisoning studies [44, 45], but SSZ is less available and therefore more expensive and seems to be less stable at high temperatures [36, 46].

Cathode

The requirements for a SOFC cathode are similar to those put on the anode, but the stability in an oxidizing environment.

Under various oxide electrodes of the perovskite structure, lanthanum strontium man-

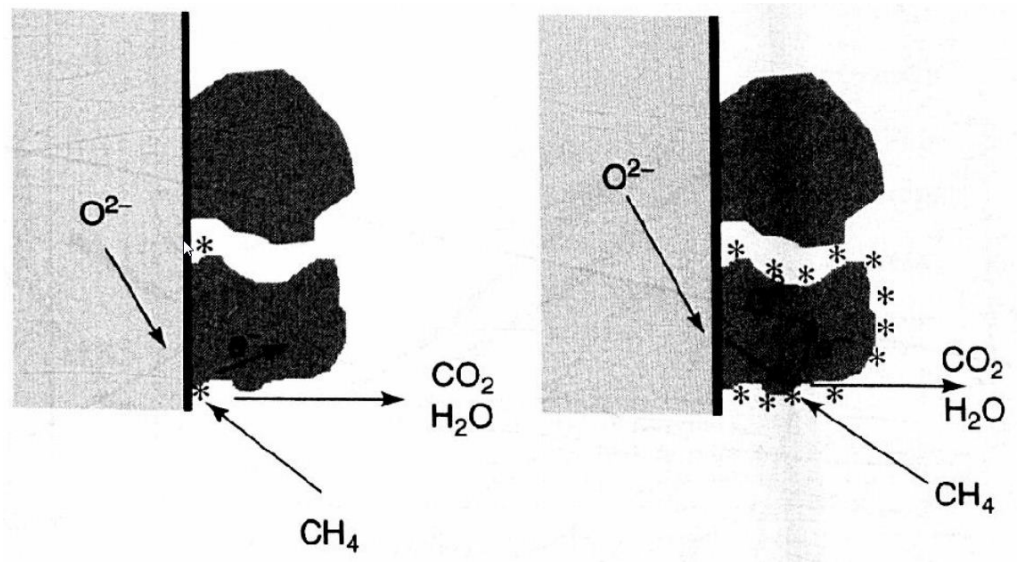

Figure 2.8: Schematic of a Ni–YSZ anode, with (right) and without (left) ionic conductance [43]

ganite (LSM, Sr-doped $La_{1-x}Sr_xMnO_3$, with x up to 30 % [47]) and lanthanum strontium cobalt ferrite (LSCF) were found to be the materials of choice. Since LSM is a good electronic conductor only, a compositional material of LSM and YSZ improves the electrode's performance. A degradation mechanism of significant concern is chromium poisoning when using chromium alloys in the adjacent materials (interconnect) [47]. A little excess of manganese (about 10 %) in LSM prevents reactions with YSZ forming insulating layers of $La_2Zr_2O_7$ and $SrZrO_3$ [37].

The usage of LSCF allows reasonable SOFC operation at temperatures down to 600 °C. LSCF ($La_{1-x}Sr_xCo_{1-y}Fe_yO_{3-\delta}$) offers both electronic and oxide ion conductivity, but is instable [47]. Without any buffer layer LSCF would react with YSZ forming insulating layers, hence a layer of gadolinia-doped ceria is used (GDC, also known as CGO for cerium gadolinium oxide) [48]. LSC ($La_{1-x}Sr_xCoO_3$) would be an even less stable alternative to LSCF with better conductivity characteristics.

In perovskite structures oxygen ions are conducted by oxygen vacancies. Polycrystalline layers are formed during the fabrication processes and mostly thin cathode layers (CFL) are applied. Cathode supported cells can rarely be found [26].

2.3.3 Fuel gases

One of the most important advantages of solid oxide fuel cells is its possibility to use a variety of fuels. This is possible due to the high temperature and to the fact that the electrolyte is an oxide ion conductor. It is clearly identified that both hydrogen and carbon monoxide can be used directly as fuel in a SOFC anode showing the following electrochemical reactions [18].

$$\mathrm{H_2 + O^{2-} \longrightarrow H_2O + 2\,e^-} \tag{2.40}$$

$$\mathrm{CO + O^{2-} \longrightarrow CO_2 + 2\,e^-} \tag{2.41}$$

It is not ascertained if hydrocarbons can react directly with the oxide ions at the triple phase boundary or if they are reformed at the anode before reacting electrochemically. Maybe both reaction paths take place at the same time [18].

A lot of studies have been undertaken to investigate methane reforming at SOFC anodes under various conditions yielding different reactions (e.g. [49], see chapter 4). Some important reactions and possible reactions steps out of a big variety are explained in the following. If enough catalyst surface and amount of water vapour is available, the steam reforming reaction takes an important role:

$$\mathrm{CH_4 + H_2O \longrightarrow CO + 3\,H_2} \tag{2.42}$$

A possible reaction in a carbon dioxide enriched environment is the $\mathrm{CH_4}$-$\mathrm{CO_2}$ reformation

$$\mathrm{CH_4 + CO_2 \longrightarrow 2\,CO + 2\,H_2} \quad , \tag{2.43}$$

another reaction occuring at an SOFC anode is direct decomposing of methane (or analogous the cracking of higher hydrocarbons).

$$\mathrm{CH_4 \longrightarrow C + 2\,H_2} \quad . \tag{2.44}$$

It is not exactly clarified when this and other reactions lead to carbon deposition. Carbon deposition arises in different forms and its occurence and form is depending on many different influences and effects like the gas composition – attention is often drawn to the steam to carbon ratio (S/C) – , the catalyst and its support, porosity and temperature. Carbon deposition can lead to deactivation of the catalyst and to decreased diffusion by blocking of pores [18].

Overall cell reaction	Temperature 25 °C	600 °C	700 °C	800 °C
$H_2 + \frac{1}{2} O_2 \longrightarrow H_2O(g)$	1.175 V	1.010 V	0.975 V	0.939 V
$CH_4 + 2\,O_2 \longrightarrow CO_2 + 2\,H_2O(g)$	1.027 V	1.006 V	1.004 V	1.003 V

Table 2.1: Calculated OCVs by means of the Nernst-equation, assumed pure fuel at the anode and air at the cathode at standard pressure (used thermodynamic data from [2, 50])

2.3.4 SOFC cell voltage

By using the Nernst-equation (equation 2.13) expected open circuit voltages (OCVs) can be calculated. In table 2.1 the Nernst-equation has been evaluated for different species and temperatures.

In order to derive an expected cell voltage of a fuel cell for gas mixtures, one can calculate the equilibrium concentrations for the given conditions and use the Nernst-equation (equation 2.13) for any of the compounds (all calculations should give the same voltage), e.g. for the direct electrochemical reaction of methane

$$CH_4 + 2\,O_2 \longrightarrow CO_2 + 2\,H_2O \tag{2.45}$$

the Nernst equation gives

$$U_{\text{Nernst}} = U^0_{\text{Nernst}} - \frac{RT}{nF} \ln \frac{p_{CO_2} p^2_{H_2O}}{p_{CH_4} p^2_{O_2}} \quad . \tag{2.46}$$

A perhaps more descriptive term for the same cell voltage can also be stated in terms of the oxygen partial pressures at the electrodes, which can be described as the driving force for the fuel cell, regardless of the fuel used [18].

$$U_{\text{Nernst}} = \frac{RT}{4F} \ln \frac{p_{O_2,\text{cathode}}}{p_{O_2,\text{anode}}} \tag{2.47}$$

Under operation oxide ions move driven by the electrochemical potential difference. They move from the cathode, where the oxygen partial pressure may be dropping at the reaction sites, to the anode, where $p(O_2)$ is rising, lowering the cell voltage.

During operation, the voltage is further decreased departing from the Nernst-voltage. See section 2.1.2 for information about those losses in fuel cell operation.

The effect of water vapour in the fuel on the electrochemical reactions (besides reform-

ing) is not totally clear. Miao et al. [51] reported a decrease in concentration polarization with 10 % of H_2O in H_2 which could be explained by a higher surface exchange rate of oxygen ions via the reaction

$$H_2O_{ad} + O^{2-}\,(\text{in YSZ}) = 2\,OH^-\,(\text{on YSZ}) \quad . \tag{2.48}$$

3 Auxiliary power unit program at AVL

This master thesis is done in the course of a project in which an auxiliary power unit (APU) is developed at *AVL List GmbH*. The APU is fueled with diesel and aimed for use in heavy duty trucks.

On trucks a lot of power is used (cooling, heating and electric appliances in the driver's cab) during the mandatory rest periods (usually overnight). This summs up to a high electric load. Therefore usually the truck engine is idling the whole rest period wasting fuel due to inefficiency, emitting plenty of particles and noxious emissions and causing noise pollution. The SOFC-APU is able to provide improvements in all points. The development is further pushed by the necessity to be in line with the future US emission regulations. SOFC technology allows fueling with diesel, which is already on-board. This way effort, costs, weight and development of further equipment can be saved [52, 53].

The targets of the APU are an electric power output of 3 kW and a total efficiency of 35 %. As a part of the durability and reliability development process, single cell testing is carried out. Both the stacks and the single cells are provided by *Topsoe Fuel Cell A/S*.

The *AVL*-APU design consists of 3 main parts (see figure 3.2). On the left there is the fuel and gas supply consisting of fuel pumps, a cathode air blower (blue), an anode gas recirculation blower (orange, working up to 500 °C and reaching an efficiency greater than 50 %) and some valves. The second part in the middle is the gas processing unit. It integrates a burner for heating at startup, a catalytic diesel reformer, a heat exchanger and an oxidation catalyst to clean the exhaust gas. The third part on the right is the SOFC stack which will be extended in future to contain 2 stacks in order to deliver the targeted power.

Figure 3.1 shows a process diagram of the APU with some values obtained by simulation, figure 3.3 shows the APU on a test stand.

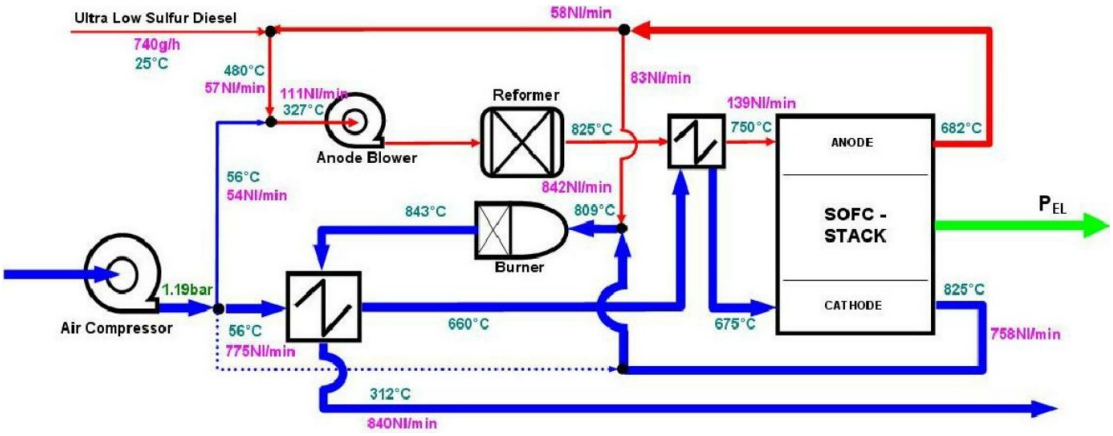

Figure 3.1: *AVL* APU process diagram with simulation results [54]

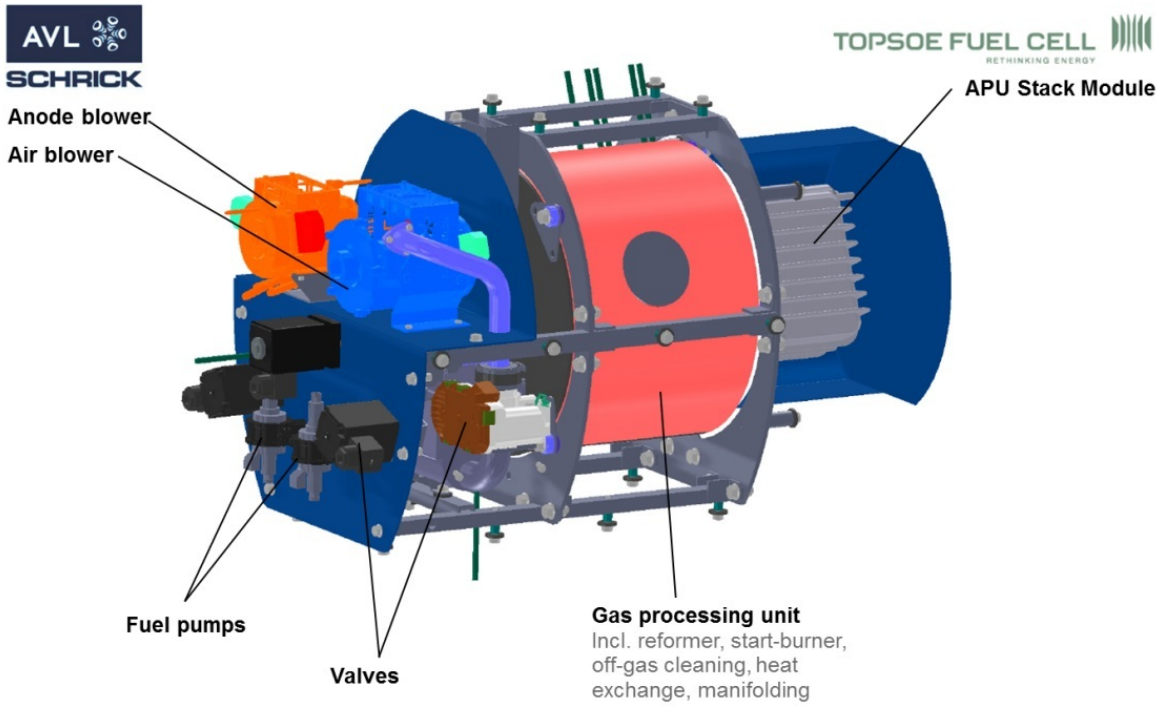

Figure 3.2: *AVL* APU drawing [53]

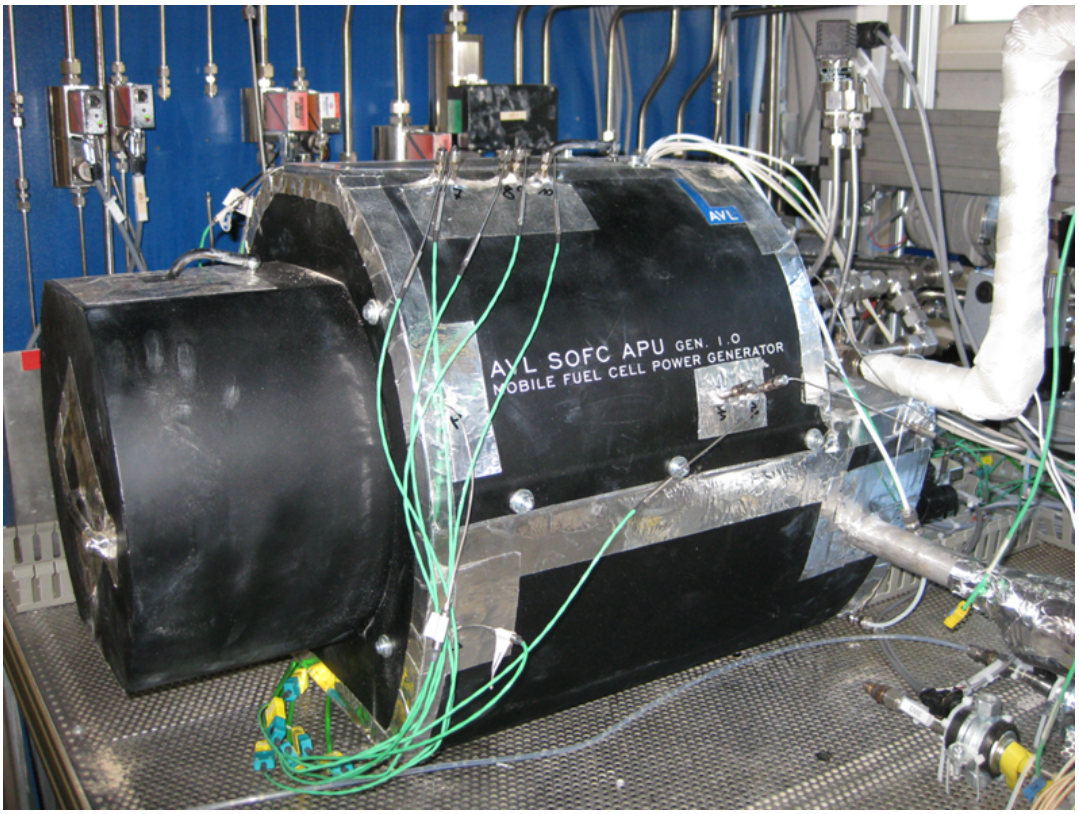

Figure 3.3: *AVL* APU Gen.I on test rig, picture from reverse side of figure 3.2 [53]

4 Sulfur poisoning

Sulfur compounds are present in a big part of fuels used in SOFCs. They are present in different concentrations in most sources related to fossil fuel as coal gas, natural gas as well as in fuels typically used in motor vehicles like diesel. In the EU and the US road diesel fuels are regulated by norms which currently allow 15ppm respectively 10ppm of sulfur in the fuel [55, 56]. Futhermore it is added to natural gas as an odour for security reasons.

Sulfur compounds reaching the anode are almost only H_2S and SO_2 compounds as present in gaseous fuels. Liquid fuels and its sulfur compounds are previously converted in reforming reactions yielding again in contained H_2S and SO_2 compounds [26].

The mechanisms of sulfur poisoning of nickel catalysts in SOFC anodes are not totally clear. At SOFC operating conditions with H_2S concentrations in the mentioned order no bulk reaction seems to take place, but chemisorption on the nickel surface takes place [57], which can be explained by the isosteric heat of adsorption (155 kJ/mol, decreasing slowly with increasing surface coverage) which was found to be significantly higher than the heat of formation of bulk sulfide (75 kJ/mol of S) [15].

$$H_2S + Ni \longrightarrow Ni{-}S + H_2 \tag{4.1}$$

The equilibrium coverage of the nickel surface by sulfur depending on temperature und the $p(H_2S)/p(H_2)$ ratio is shown in figure 4.1. Regeneration from sulfur poisoning should be possible in a pure hydrogen fuel stream, but it takes a long time. Accelerating the regeneration with the help of water vapour in the stream is possible only close to the catalyst oxidation equilibrium constant, which is dangerous for nickel catalysts [15].

Sulfur in the form of SO_2 is considered to be no problem for SOFC anodes because no direct adsorption onto the nickel surface is expected. Sulfur deposition could occur in the presence of both SO_2 and H_2S via the reaction

$$2\,H_2S(g) + SO_2(g) \longrightarrow 3\,S(s) + 2\,H_2O \tag{4.2}$$

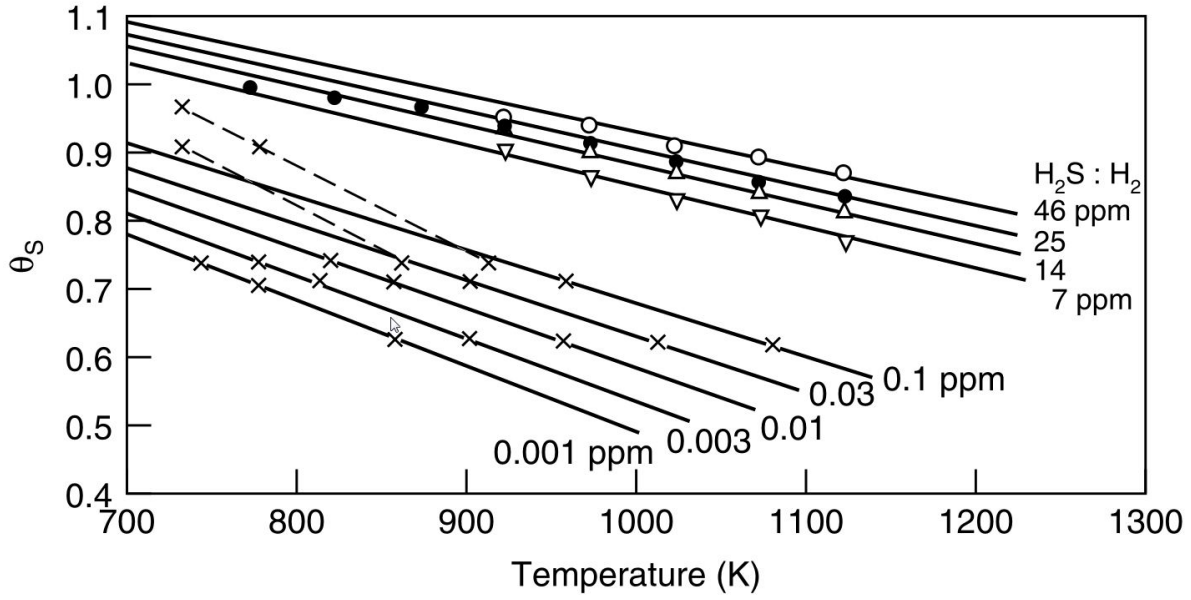

Figure 4.1: Sulfur surface coverage for nickel in H_2S

or by way of convertion of SO_2 to H_2S [26].

Under equilibrium conditions almost all sulfur compounds should be converted to H_2S via the reaction

$$2\,H_2O + H_2S \rightleftharpoons SO_2 + 3\,H_2 \tag{4.3}$$

with the equilibrium constant K in the range of 2.8×10^{-11} to 2.3×10^{-5} at 1 bar at 500 °C to 1000 °C. So under equilibrium conditions only the amount of sulfur in the fuel stream may be crucial [15], which is investigated by Rittenschober for the conditions of this study [54].

Some points of the influence of sulfur on solid oxide fuel cells are widely agreed on [15]:

- the influence of sulfur is higher at lower temperatures
- it is lower at higher current densities (the effect of sulfur should be related to increase in cell resistance, because unclarities could arise when galvanostatic and potentiostatic modes are compared [58])
- regeneration is faster with current drawn

The first point can be explained by increased mobility of all compounds including sulfur at elevated temperatures. An experimentally supported correlation between the coverage

of sulfur on a nickel surface and temperature at different H_2S concentrations is suggested to be described by

$$\Theta_S = 1.45 - 9.53 * 10^{-5}T + 4.17 * 10^{-5}T * \ln(\frac{p(H_2S)}{p(H_2)}) \qquad [15]. \tag{4.4}$$

The causes for the second and third point are not so clear, but may be explained by measured decreased H_2S contents at the anode outlet which may indicate a conversion of the chemisorbed sulfur to SO_2 by the following reactions [59].

$$H_2S + 3\,O_2^- \longrightarrow SO_2 + H_2O + 6\,e^- \tag{4.5}$$

$$H_2S + 2\,H_2O \longrightarrow SO_2 + 6\,H_2 \tag{4.6}$$

Many research groups made investigations on sulfur poisoning of SOFCs fueled with hydrogen, but since there are a lot cross influences by several parameters, the results are very specific. Only in recent years more studies haven been made on ASC cells, which show a different sulfur poisoning behaviour [60]. Often higher H_2S contents are investigated and various fuel compositions are tested. Other studies treat the matter of alternative materials like SSZ which are more sulfur tolerant.

To some extent it is tried to differentiate between the effects of sulfur poisoning on electrochemical reactions and on pure reforming reactions, because it is suggested that the sites for electrochemical and for catalytic conversion in a SOFC appear not to be the same [59]. Nevertheless most research groups are describing the effect on the whole SOFC cell under operation.

4.1 Impact on SOFC operation

On first contact of sulfur to Ni-YSZ anodes an immediate drop of the cell voltage is reported (first order degradation), which is clearly assigned to nickel surface coverage. A possible additional effect is an electrostatic effect due to the high electronegativity of the sulfur atoms on the nickel surface. Then a less steep gradual decrease on the long time scale (second order degradation) is observed [44, 60–62]. A possible explanation for the gradual degradation is that continued sulfur exposure leads to surface reconstruction of nickel or possible interactions between sulfur and the electrolyte [61, 62]. Interestingly Lussier et al. [62] found a performance increase under H_2S exposure on a cell which had completely ceased to function proposing a restored electronic conductivity by formed

nickel sulfide as a possible mechanism.

Yang et al. [60] compared sulfur poisoning of ASC and ESC cells, stating a significantly longer duration of first order degradation to occur on ASC cells. Furthermore, they found the sulfur poisoning (measured by means of the relative cell resistance change) to decrease with increased current density suggesting the reaction of equation 4.6.

Matsuzaki et al. [63] tested 79 % H_2 and 21 % H_2O on a Ni-YSZ cermet elctrode and YSZ electrolyte and found degradation when the H_2S concentration exceeded 0.05, 0.5, and 2 ppm at 1023, 1173 and 1273 K, respectively. The time needed for the sulfide impurity to saturate was almost independent of the sulfide concentration and was found to be approximately 3.3, 2.5 and 1.1 hours at 750, 900 and 1000 °C, respectively. The degradation was found to be reversible in all cases (tested H_2S concentrations up to 15 ppm). The degree of sulfur-poisoning was found not to depend on the equilibrium partial pressure of S but on the total sulfur content in the fuel.

Bao et al. [11] investigated effects of various impurities found in coal gas including H_2S on SOFC performance. The synthetic fuel gas mixture contained 30.6 % H_2, 30 % CO, 11.8 % CO_2 and 27.6 % H_2O with a current density of 0.222 A/cm^2, a temperature of 750 °C and a flow rate of about 0.1 Nl/min with cell area of 4.5 cm^2 which would correlate to a flow rate of 21.3 Nl/h to the cell size used in this study. When H_2S was introduced to the cell at a level of about 0.9 ppm to 1 ppm an immediate drop in cell voltage of about 3.5 % (from 143.5 mW/cm^2 to 138.5 mW/cm^2 in constant current mode) was observed. Until the end of the test after about 100 h a gradually recovery to 141 mW/cm^2 and afterwards a complete recovery after H_2S removal from the fuel stream was reported. Furthermore, Bao et al. [12] studied synergistic effects with other impurities showing accerlerated cell degradation in the presence of H_2S together with arsenic, phosphor or both.

Sasaki et al. [44] measured the cell voltage drop as a function of the H_2/CO ratio of fuel gases containing 5ppm H_2S on cells with Ni/YSZ anodes and YSZ electrolyte. They observed a relatively stable voltage drop up to ratios of about 20:80 and a rapidly decreasing voltage at above 90% CO, but unfortunately neither information on fuel humidification nor on fuel utilisation is clear.

Various reactions occuring in SOFCs were studied by Kuhn et al. [49] under the influence of H_2S. They found the steam reforming and water-gas-shift reactions much more prone to sulfur poisoning than the direct oxidation reactions of CH_4 and CO. Furthermore H_2S is suggested to strongly decrease hydrocarbon decomposition (equation 2.44) and thus decreasing carbon deposition.

4.2 Impact on reforming reactions

Hagen et al. [45] investigated the methane conversion of 4x4cm SOFC cells monitoring the in-cell voltage. Without any addition of H_2S to the fuel flow (totally 10 Nl/h) the CH_4 content was presumably converted shortly after reaching the cell. When injecting 2 ppm of H_2S the methane conversion needed a catalyst surface in the magnitude of the whole anode. When increasing to 4ppm and higher the methane conversion rate decreased to 80 % and less.

Internal methane conversion is an endothermic reaction using waste heat from the fuel cell operation which helps cooling a stack. Hence the maximum permissible stack output can be increased compared to operation with sulfur in the fuel affecting the methane conversion. However too much CH_4 in the fuel leads to high temperature gradients on the anode [15]. It has clearly been demonstrated that sulfur adsorption in the anode has a much stronger impact on the steam reforming rate than it does on the electrochemical processes. Hence slowing down of the reforming rate of methane rich fuels by controlled sulfur poisoning is an interesting technological possibility [45, 62, 64, 65].

5 Experimental design and assembling

5.1 Test setup

5.1.1 Cell housing

In this study cells were tested in a ceramic cell housing based on the *TrueXessory-HT* by *FuelCon AG*. A scheme and a picture of the cell housing are shown in figures 5.1 and 5.2.

The cell housing was designed for use with inlets for anode and cathode gas and an anode gas outlet. The cathode gas streamed out into the oven chamber shortly after passing the cell. In order to use the available furnace a ceramic socket had to be designed in the beginning of the work. The 3 gas tubes could then be glued into the socket leading into the furnace from its ceiling. Temperature sensors were glued into prepared holes at the gas channels of the socket to measure the gas temperatures before and after the cell. In order to minimize reactions with sulfur and the adsorbance at high tempereatures, the gas inlet and outlet tubes were also made of ceramic.

All ceramic parts were made out of aluminium oxide (Al_2O_3). In order to avoid high temperature gradients the heat-up and cool-down rate was set to 1 K/min and the difference between the cell and the oven temperature has been permanently observed. For glueing of all ceramic parts, the two-component adhesive Fortafix QS/B4 by *Detakta* was used. It offers a good gas tightness.

In the applied sealing concept no extra materials like glass solder were needed to seal the electrode chambers. Gas tight seals were attained at plane ceramic faces. Since SOFC electrodes are porous, sealing was made at the electrolyte surface. Therefore the cells, which had a total size of 5 x 5 cm, had a cathode size (and active area) of 4 x 4 cm. The uncovered part of the electroyte was pressed onto a face of the lower ceramic housing part (see figure 5.1). So the anode and the cathode chambers were separeted and gas was not able to permeate from one to the other. An additional weight (not drawn in figure 5.1) was put onto the upper part of the ceramic housing to improve

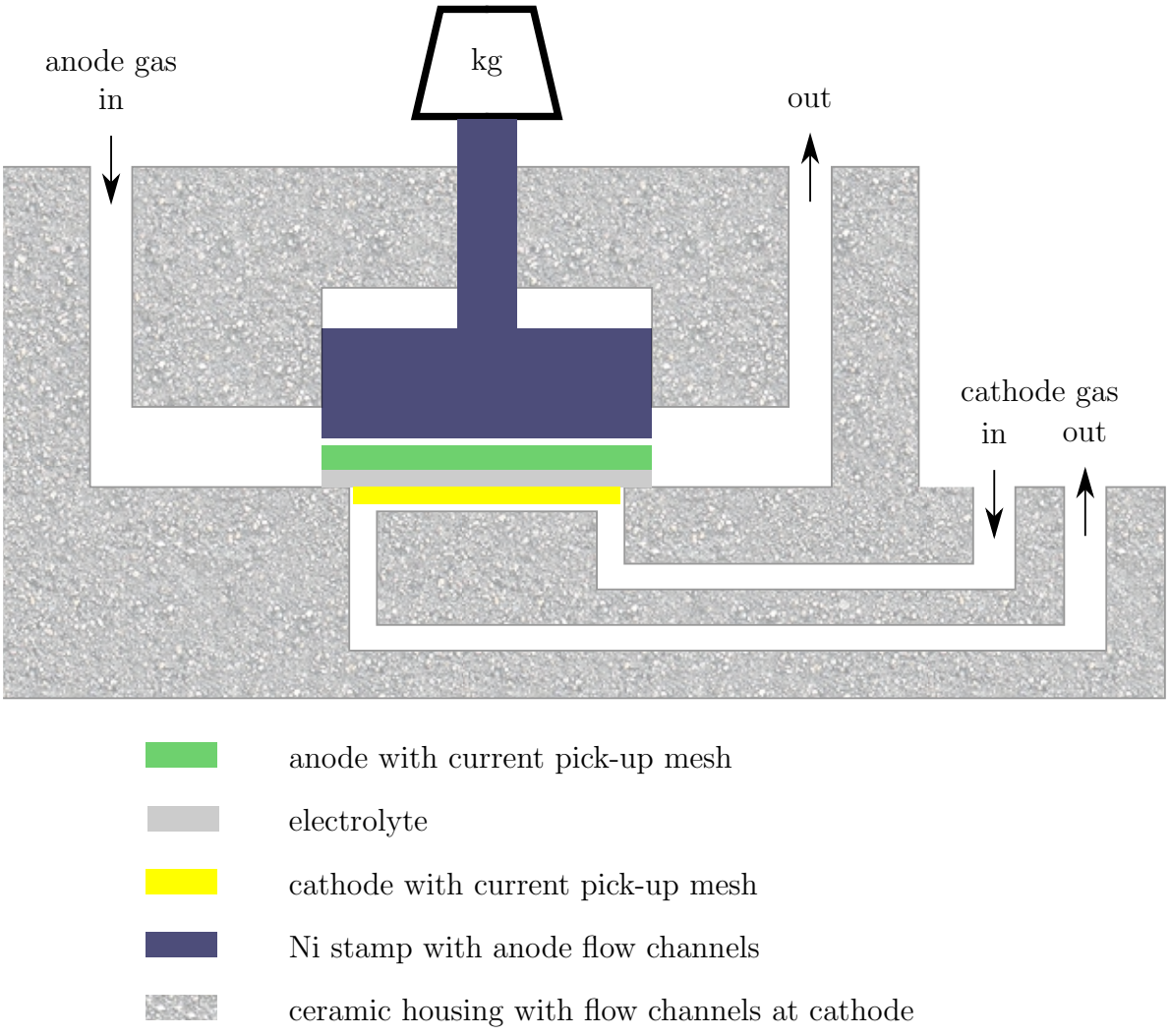

Figure 5.1: Scheme of the cell housing, the drawn weight is improving electrical contacts and the sealing between the anode and the cathode chambers

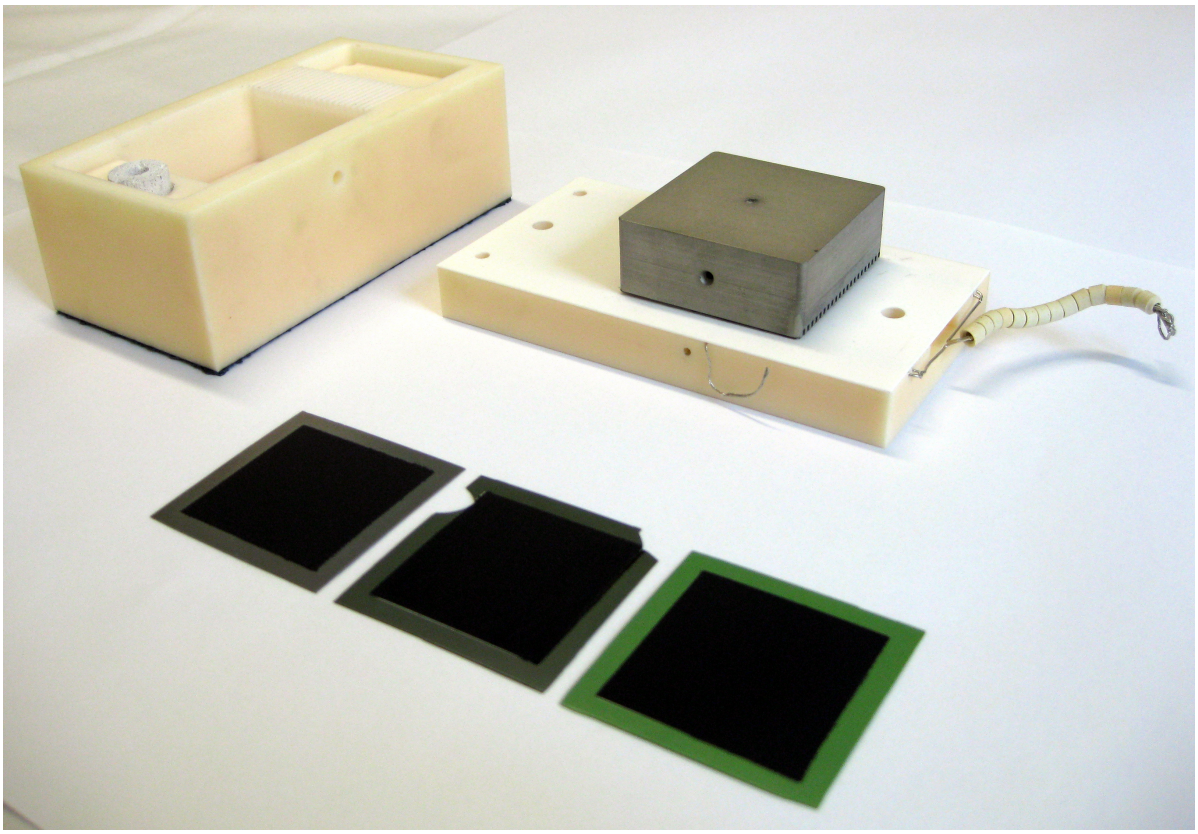

Figure 5.2: SOFC cells (cathode side, with the exposed electrolyte on the edge) and parts of the cell housing with the anode chamber opened; the sealing is established by pressing the plane ceramic faces together; flow channels can be seen at the bottom of the nickel stamp

the gas tightness between the electrode chambers and the outside (the opened anode chamber is shown in figure 5.2.

On top of the anode a fine and a coarse nickel mesh were used for electrical contact to the electrode. The nets were pressed onto the cell by a nickel stamp with a bar reaching to the outside of the furnace, which had a weight mounted on top of it (figure 5.1). At the cathode side platinum meshes were used for the electrical contact. The pressure by the weight was used for good electrical contact at both electrodes and the sealing at the electrolyte edge. Therefore the thickness of the cathode meshes had to be adjusted to the cathode thickness and the available space. The weight was about 7 kg. An electrical 4 point measurement was carried out. The nickel stamp was contacted by a platinum sense wire and the thick bar made out of inconel 600 as a working wire. At the cathode the coarse mesh had 2 thick lines connected to another inconel bar leading the cathode current to the outside of the oven and a thin wire connected to the platinum cathode sense wire. The two sense wires leading to the outside of the oven were electrically isolated with ceramic bushings.

The incoming anode gas mixture was going through a porous ceramic plug to avoid turbulent flows before reaching the flow channels which are build into the nickel stamp. The cathode gas stream was led through flow channels built into the ceramic part underneath the cell. In figure 5.1 the flow channels are illustrated by the thin gaps next to the electrodes. The fuel and oxidant gases flowed into opposite directions (counter flow).

In order to minimize gas leaking, any dirt and even the most minute displacement of any of the components had to be avoided. The various ceramic cell housing layers, the meshes and the cell itself were set up in the furnace using plastic gloves.

A temperature sensor was installed into drill holes in the lower ceramic part just underneath the cathode flow channels to measuring the cell temperature.

5.1.2 Test stand

The test stand included the gas supply system, the furnace, which contained the cell housing, various sensors, an electronic load, an interface for hardware and measurement control connected to a computer for user control and data logging.

The test gases were supplied using mass flow controllers. The layout of the gas supply system is shown in figure 5.3. One mass flow controller was of the type *EL-FLOW* by *Bronkhorst High-Tech B.V.* and all others were of the type *red-y* by *Vögtlin Instruments AG*. Due to the failure of a mass flow controller, the standard test parameters had to

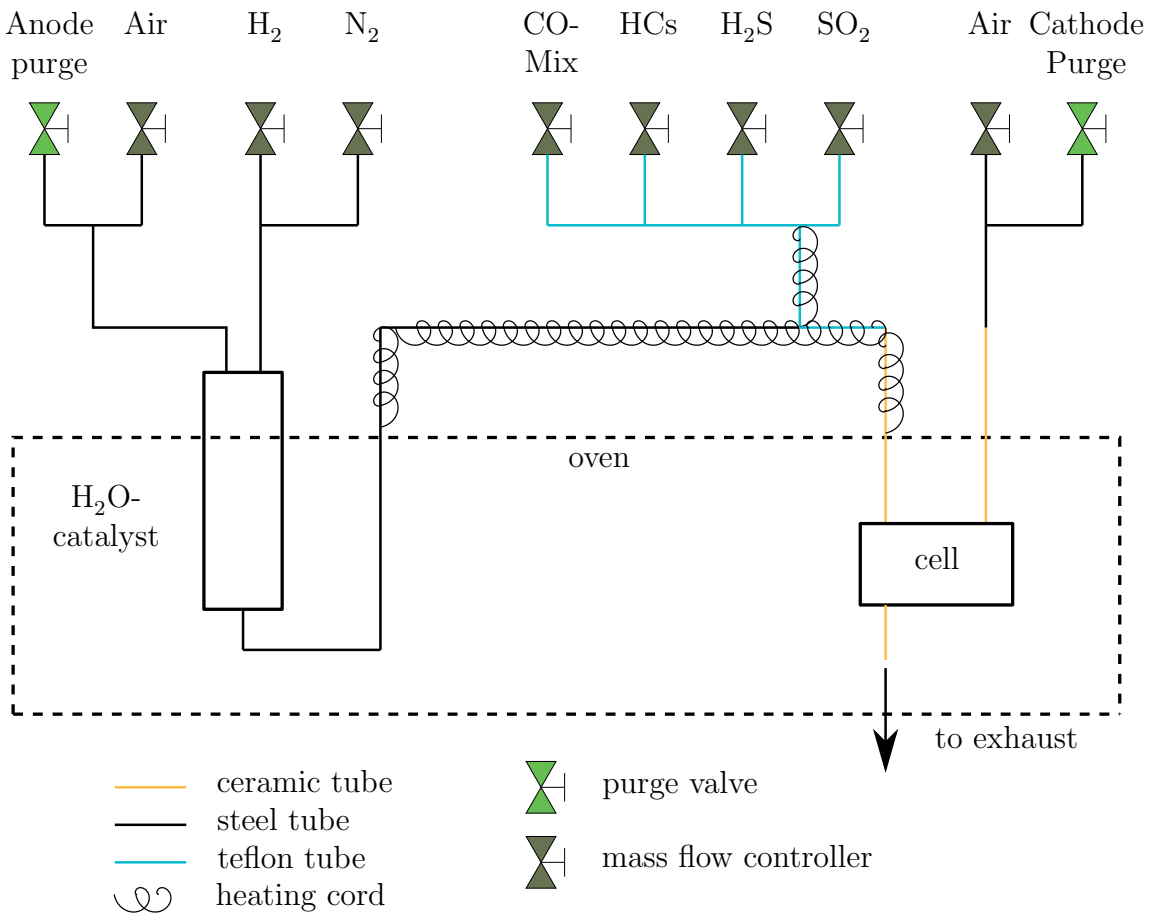

Figure 5.3: Scheme of the gas supply system, the cathode gas is released into the oven chamber after passing the cell

be changed for a single test (see section 6.2). The controller was then changed, but the flow rate for the following regeneration periods had to be changed (see section 6.1). Furthermore, one controller showed irregularities resulting in small voltage jumps every now and then (e.g. as shown in figure 6.4(a)).

The water vapour for the anode gas stream was produced at the test stand by mixing air with excess hydrogen and nitrogen. Those two gas flows were led into the furnace concentrically into the 'H_2O-catalyst', where they were brought together shortly before a nickel mesh to obtain a steady oxidation. Then the other anode gas components were added. Different humidification systems were subject to testing beforehand (see section 5.1.3).

At both anode and cathode purge valves were installed for safety reasons. During a possible failure of the gas supply system (e.g. due to a power blackout) a gas mix of 9 %

H_2 in N_2 was available for the anode and air for the cathode. That way damage of the cell due to starvation or reoxidation of the anode could be ruled out.

The temperature of the gas stream was held above 100 °C to prevent the water vapour from condensing. Heating cords by *Horst GmbH* were used. In order to minimize sulfur adsorption in the gas suppy system, the sulfur containing part of the gas supply system was made of PTFE (Teflon) tubes connected to the ceramic tubes leading into the furnace to the cell housing.

Thermocouples of type K were used to monitor several temperatures in the test setup. The temperature measurement in the cell housing socket showed that the gas streams reached the oven temperature at all applied flow rates before coming to the cell.

The furnace was of the type *Kammerofen* by *HTM Reetz GmbH* with a maximum temperature of $T_{\max} = 1000\,°C$.

The electronic load *ZS3612* by *Höcherl und Hackl* was used. Two thick working wires were screwed onto the inconel bars reaching out of the oven from the cell housing and two thinner copper cables were connected to the platinum sense wires (described in section 5.1.1). During the tests the current was set to a constant value and the voltage was measured. So the electronic load was operated in constant current mode (galvanostatic mode).

For experimental control a generic *Labview* program for the SOFC oven testbed was available at *AVL*. It was adapted for the single cell testing and its components. The whole equipment for experimental control and measurement was connected to the control computer either directly or via an additional hardware interface.

5.1.3 Humidification tests

For the single cell tests a humidified anode gas stream was required. The water vapour delivery system had to work properly with rates in the range of down to 0.69 g/h. Therefore neither a bubbler system nor a water pump with an evaporator could be used. Those systems would have been operating too inaccurately. An approach of mixing air (the flow rate controlled by an additional mass flow controller at the anode side) to the anode gas was pursued. The fed oxygen should be completely converted with hydrogen into water vapour. The reaction of oxygen with hydrogen should yield an oxygen partial pressure $p(O_2) < 10^{-21}$ at $T = 500\,°C$ with only 1 % more hydrogen than the stoichiometric amount.

Firstly the mixed gas stream was led through a heated platinum-rich catalyst (*protonics C-type*, by *Umicore*, figures 5.5) at temperatures from 500 °C to 700 °C. The output

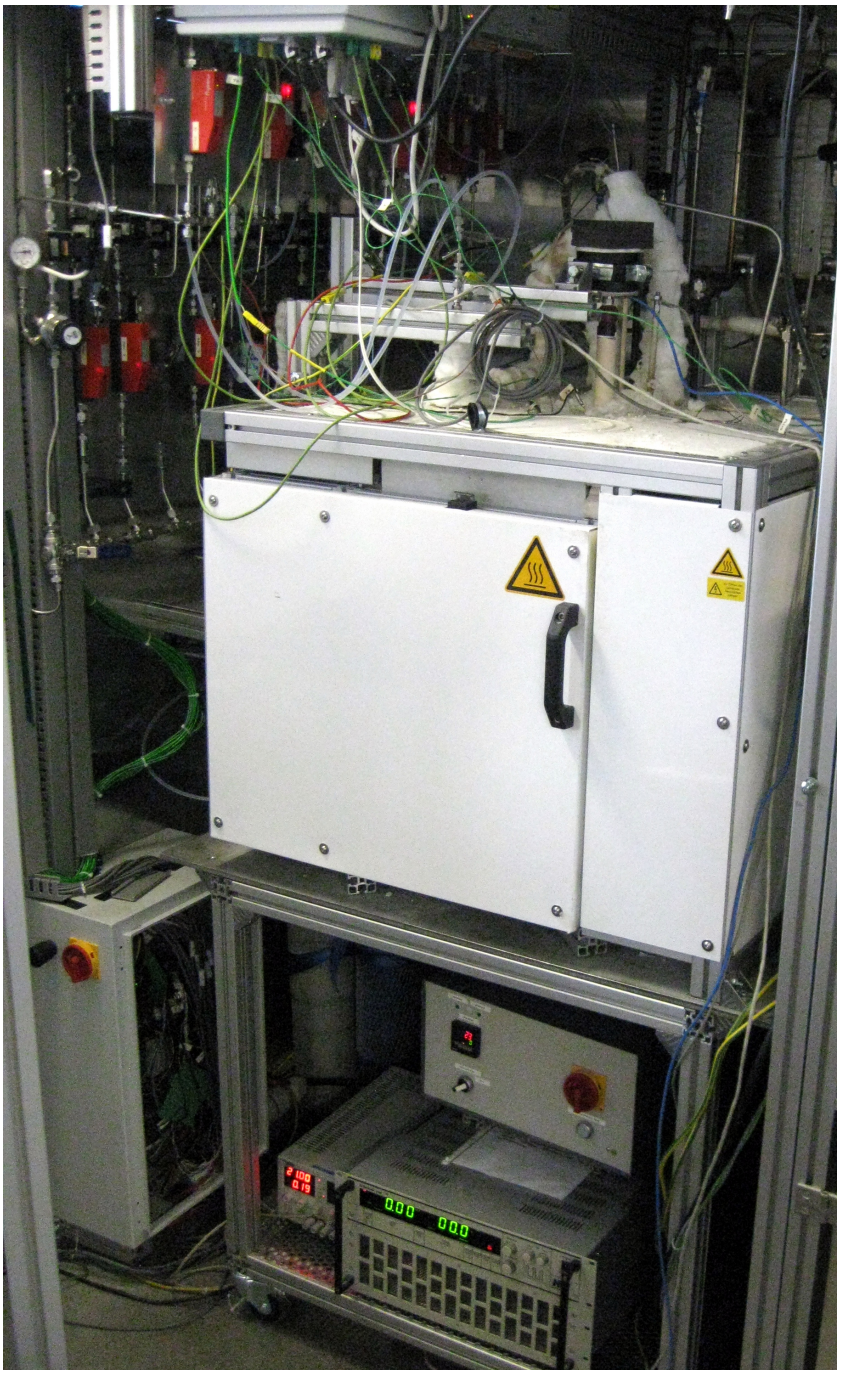

Figure 5.4: Test stand; including furnace, underneath the furnace controller, the electronic load (green digits) and a power supply for SOEC operation (red digits) at the bottom, a electrical control box at the lower left (opened), the gas supply system at the upper left and T-sensors, electric wires and the anode weight above the oven

Figure 5.5: Catalyst after use in humdification tests for the anode gas stream, a heating cord is wrapped around the pipe, and a temperature sensor reaching into the gas stream is visible in front of the catalyst

gas composition was then analyzed with a gas chromatograph (*Agilent Technologies 490 Micro GC*) and indicated remaining O_2 in the anode stream. Later it turned out that the GC was not working properly due to defects or gas leakages.

New measurements were then conducted with steel wool in the pipe in front of the catalyst to improve the mixing of the gas (figure 5.6). The GC wrongly indicated that oxygen was still remaining in the order of 100 ppm, which is too much for a SOFC anode gas. A possibility for an incomplete reaction was a still insufficient mixing of H_2 and O_2 due to the low flow velocity and the short path to the catalyst. Therefore the path was extended and twisted for a better mixing. Other assumptions for the once again unpleasant GC-measurements were the damage of the catalyst due to very high local temperature and a possible flashback of flames resulting in an intermittent and incomplete reaction.

Then the error in the GC device was found and the humidification system as described in the previous section was applied. The OCVs measured when operating SOFC cells showed that the humidification system worked well.

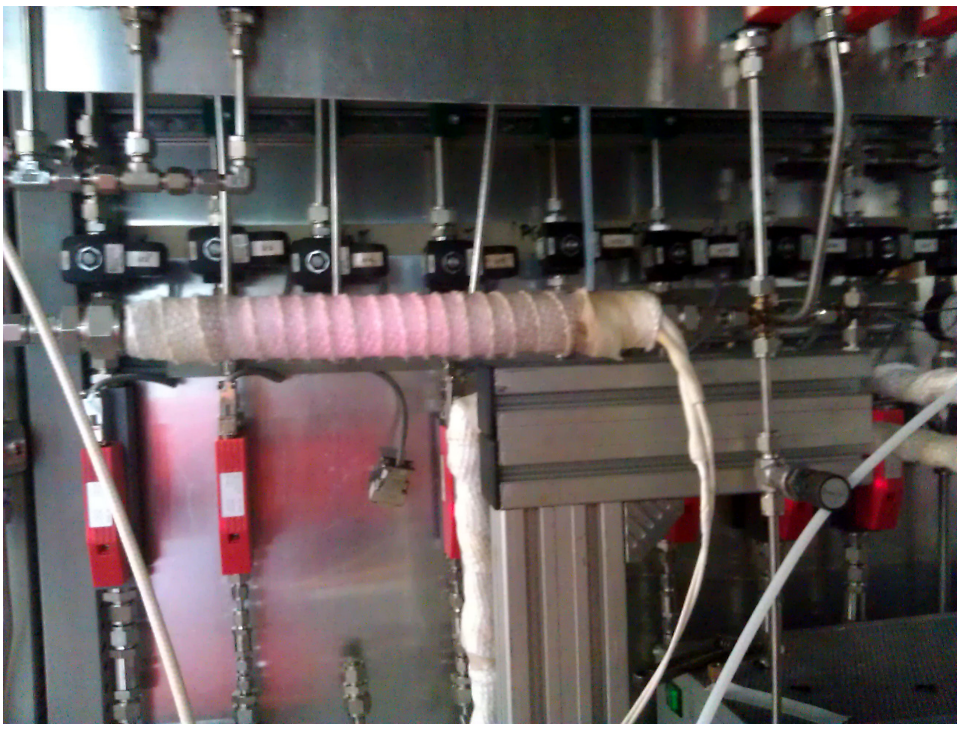

Figure 5.6: Testing of the humidification for the anode gas stream, the outlet of the heated pipe is connected to a GC

5.2 Start-up tests and procedures

Electrical tests were carried out to minimize measurement errors and to ensure safety. The grounding of the furnace and all other components was tested and, where necessary, established. The conductivities of the 4 measurement lines and their insulations to all other conducting parts of the test tig were tested with a handheld multimeter at room temperature and after heatup.

Gas leakage tests were carried out at both room and operating temperature. The gas tightness of all metal and PTFE components of the gas supply was succesfully tested with high pressure. The pressure in the anode chamber of the cell housing could not be greatly increased, because otherwise the upper part of the cell housing was lifted. An additional weight of 3 kg was put onto the housing to enhance the sealing from the electrodes to the outside. The maximum gauge pressure before the cell housing is lifted is calculated to

$$p = \frac{g * m}{A} \sim 50\,\text{mbar} \qquad , \tag{5.1}$$

where A is the area of the cell housing, m is the weight pressing on the sealing faces and g is the earth's acceleration. The other weight was raised to about 7 kg to ensure gas

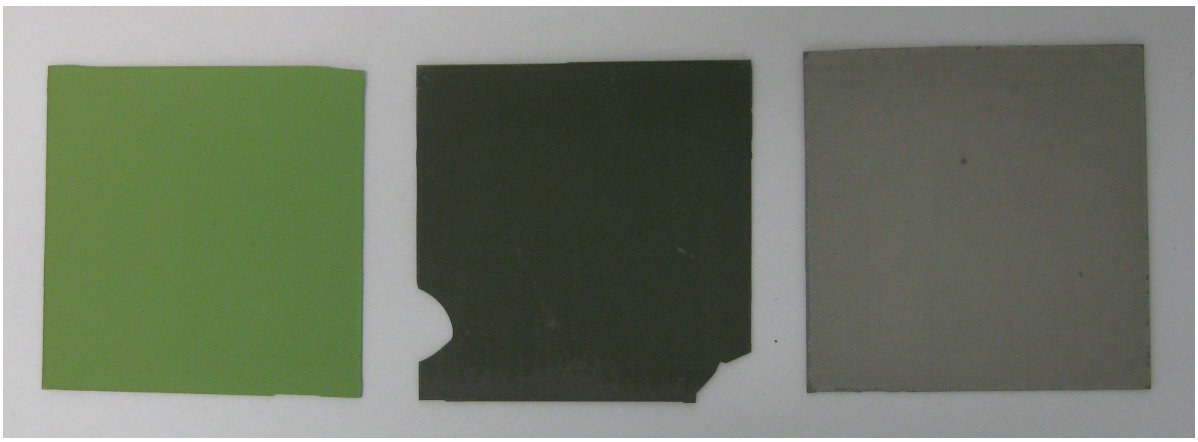

Figure 5.7: Picture of the anode sides of 3 cells, left: new and unused cell, middle: used cell with air contact at cooldown (damaged at disassembly), right: used cell cooled down in H_2 environment

tightness between the anode and the cathode.

It is sure that anode gas leaks out of the cell housing to some amount, but the gage pressure at the anode during operation was always below 10 mbar. Therefore this loss was neglected. After the oven was heated up, the hydrogen leakage before entering the oven in ceramic tubes was tested. A hydrogen stream was set and a handheld gas sensor was used near the tubes, indicating a maximum H_2 concentration of about 40 ppm close to the thermal insulation of the gas tubes. Those leakages are presumably located at the transition from the PTFE to the ceramic tube and have minor impact on the fuel utilisation, only.

The new SOFC cells were delivered with oxidized anodes (greenish NiO, left cell in figure 5.7). The activation (reduction procedure) of the cells was done as specified by the manufacturer. A cathode flow of 40 Nl/h air and a anode flow of 20 Nl/h of 9 % H_2 in N_2 were set. The temperature was then risen from room temperature to 835 °C at a rate of 1 K/min. These conditions were kept for 2 h. Then the anode gas composition was changed to pure H_2 and held for 1 h, the cathode flow was set to 100 Nl/h, a current of the standard rate ($I = 2.72$ A) was set and the temperature was reduced to the standard temperature 735 °C. The standard values refer to the test matrix described in the next section.

The first cell was prepared for testing, the reduction procedure was carried out and the cell reached a stable voltage. When the humidification was turned on, the heating cords, which prevent condensation of water, destroyed the PTFE-tubes of the anode gas stream. The cell got contact to air at 735 °C, therefore it was most likely damaged. The

slightly greenish nickel oxide (NiO) can be seen in figure 5.7 (middle cell).

During the reduction procedure of the second cell, a device was connected in a wrong way to the cell voltage circuit, so some current was drawn from the cell during heat up. The undefined current was lower than the standard testing current of 2.72 A and did not seem to have any impact on the cell. The cell was then investigated in electrolysis mode (SOEC mode, solide oxide electrolysis cell). Water vapour and hydrogen were used at the anode only and air flowed through the cathode to remove produced oxygen. The SOEC tests were done by Wede and are described in [66]. The cell was running for approximately 260 h. Then the reference tests were conducted before the first sulfur tests started.

Sulfur adsorption was expected to appear on all parts of the anode path. Due to the small sulfur concentration it may take many hours until sulfur reaches the cell for the first time, because it is adsorbed in the path of the anode gas. In all following tests the adsoption equilibrium should be established rapidly [67]. A duration of 45 min was reported by Bao [11] at a concentration of 1 ppm. Using this test setup it took about 2 h with a sulfur concentration of 0.29 ppm until any reaction in cell voltage could be measured [54].

5.3 Test matrix

Measurements according to a test matrix were conducted where in each test a certain parameter was changed in order to evaluate the effect of this change. In fuel cell operation most effects cannot be isolated, but are related to each other. Hence it is not always possible to get unambiguous insights. Starting point of the tests were the standard parameters shown in table 5.1. The fuel utilisation stated in this table was calculated assuming full conversion of all hydrocarbon compounds. The composition of the hydrocarbon-mix and the CO-CO_2-mix are stated in tables 5.2 and 5.3. The full

c(H_2)	c(H_2O)	c(CO)	c(CO_2)
16.5 vol%	10.7 vol%	14.2 vol%	10.1 vol%
c(H_2S)	c(SO_2)	c(HC-mix)	c(N_2)
0.25 ppm	0.29 ppm	738 ppm	48.4 vol%
I	η_{fu}	T	total anode flow
170 A/cm^2	20.7 %	735 °C	17.74 Nl/h

Table 5.1: Standard test parameters

CH_4	66.7 %
C_2H_4	11.7 %
C_2H_6	3.9 %
C_3H_6	17.8 %

Table 5.2: Composition of the hydrocarbon mix, for easier flow rate controlling the mixture was diluted in nitrogen

CO	58.32 %
CO_2	41.68 %

Table 5.3: Composition of the CO-CO_2-mix, the mix was diluted with hydrogen in a gas pressure cylinder

test matrix (partly done by Rittenschober [54]) is shown in table 5.4.

At the very beginning and after each test a regeneration period with pure hydrogen as fuel was carried out. In order to accelerate regeneration a current density of the standard value (170 A/cm^2) was set. The durations of these periods were at least 9 hours and ended when the voltage came to a stable value. I-V-curves were recorded at the end of each regeneration period. Due to a problem with a mass flow controller the H_2 regeneration flow was set down from the standard flow of 17.74 Nl/h to 12 Nl/h starting with the regeneration period after the hydrocarbon test.

The electronic load sometimes did not always keep the current completely stable, but ripples can be seen in the current graphs (e.g. figure 6.6). The ripples have a maximum amplitude of 47 mA, which corresponds to about 3 mA/cm^2, and a periodic in the range of 35 min to 110 min. There seemed to be an issue with the electronic load setting the constant current, but it may also be a measurement error. No significant influence on the measurements was oberserved.

Voltage-current-curves were obtained by setting the current and keeping it for 30 s. Measured current and voltage values were then averaged.

All calculations of equilibrium concentrations were made with the software *Gaseq* in Version 0.79b by *Chris Morley* (`http://www.gaseq.co.uk`). Expected open circuit voltages for the case of chemical equilibrium could then be calculated using the Nernst equation.

	$c(H_2)$ [vol%]	$c(H_2S)$ [ppm]	$c(SO_2)$ [ppm]	$c(H_2O)$ [vol%]	i [mA/cm^2]	T [°C]	c(CO-CO_2-mix) [vol%]	c(HC-mix) [ppm]	c(N2) [vol%]
regeneration	100	0	0	0	0	0	0	0	0
(1) reference	100	0	0	10.7	170	735	24.3	738	48.4
regeneration	100	0	0	0	170	735	0	0	0
(2) H_2S-test[1]	16.5	0	0.29	10.7	170	735	24.3	738	48.4
	16.5	**0.25**	0.29	10.7	170	735	24.3	738	48.4
	16.5	0.97	0.29	10.7	170	735	24.3	738	48.4
regeneration	100	0	0	0	170	735		0	0
(3) SO_2-test[1]	16.5	0.25	0	10.7	170	735	24.3	738	48.4
	16.5	0.25	**0.29**	10.7	170	735	24.3	738	48.4
	16.5	0.25	0.97	10.7	170	735	24.3	738	48.4
regeneration	100	0	0	0	170	735	0	0	0
(4) CO-CO_2-test[2]	41.1	0.25	0.29	10.7	170	735	0	760	42.8
	26.5	0.25	0.29	10.7	170	735	14.6	760	42.8
	16.8	0.25	0.29	10.7	170	735	**24.3**	760	42.8
regeneration	100	0	0	0	170	735	0	0	0
(5) HC-test	16.5	0.25	0.29	10.7	170	735	24.3	358	48.4
	16.5	0.25	0.29	10.7	170	735	24.3	**738**	48.4
	16.5	0.25	0.29	10.7	170	735	24.3	1433	48.4
regeneration[3]	100	0	0	0	170	735	0	0	0
(6) H_2O-test	16.5	0.25	0.29	4.9	170	735	24.3	738	54.3
	16.5	0.25	0.29	**10.7**	170	735	24.3	738	48.4
	16.5	0.25	0.29	16	170	735	24.3	738	43.1
regeneration[3]	100	0	0	0	170	735	0	0	0
(7) current-test	16.5	0.25	0.29	10.7	0	735	24.3	738	48.4
	16.5	0.25	0.29	10.7	120	735	24.3	738	48.4
	16.5	0.25	0.29	10.7	**170**	735	24.3	738	48.4
regeneration[3]	100	0	0	0	170	735	0	0	0
(8) temperature-test	16.5	0.25	0.29	10.7	170	785	24.3	738	48.4
	16.5	0.25	0.29	10.7	170	**735**	24.3	738	48.4
	16.5	0.25	0.29	10.7	170	685	24.3	738	48.4
regeneration[3]	100	0	0	0	170	735	0	0	0
(9) reference	16.5	0	0	10.7	170	735	24.3	738	48.4

[1] tested by Rittenschober [54]
[2] standard parameters changed
[3] total flow of 12 Nl/h

Table 5.4: Test matrix, total anode flow of 17.74 Nl/h, the flow rate at the cathode was set to 100 Nl/h of air in all tests. The parameters marked yellow were varied in the respective test. The variation took place against the parameters marked orange, where applicable

6 Results and discussion

6.1 Reference tests and regeneration periods

A reference test was carried out at the very beginning of the cell tests. The cell did not have contact to any sulfur compounds before this test. After this reference measurement the first sulfur tests were conducted by Rittenschober as described in [54]. At the very end of the cell tests another reference test was performed. In both reference tests the standard fuel without any sulfur compounds was used. The graphs of the tests are shown in figure 6.1 and for comparison a reference I-V-curve is shown in the graphs of the single tests.

The cell voltage under reference conditions (current density $I = 170\,\mathrm{A/cm^2}$) cannot be determined exactly and lies in the range of 0.827 V to 0.854 V. A degradation of the cell was observed in the reference test in the beginning, while in the test at the very end the cell still regenerates from the tests done. Sulfur compounds could not be totally removed from the cell in the regeneration periods. Hence the following tests yield a faster first degree poisoning than in the previously conducted tests described in [54] when the cell had contact to H_2S for the first time.

The I-V-curves of the regeneration periods are shown in figure 6.2 together with a I-V-curve after the cell activation. The curves are listed chronologically in the legend of the figure. The I-V-curve of the regeneration period after the CO-CO_2-variation test is corrupted, because of the work done on the test stand after the failure of a mass flow controller.

The first 4 curves were obtained with a hydrogen flow rate of 17.74 Nl/h. The cell could not regenerate completely and the periods finished at lower voltages after every test. The flow rate had to be reduced to 12 Nl/h for the following 5 regeneration periods resulting in a lower voltage level. In the following the cell could be regenerated to this level after each test.

The OCV of the reference test at the beginning (measured at the end of the test period) was 980.9 mV, the one of the reference test at the end 978.3 mV.

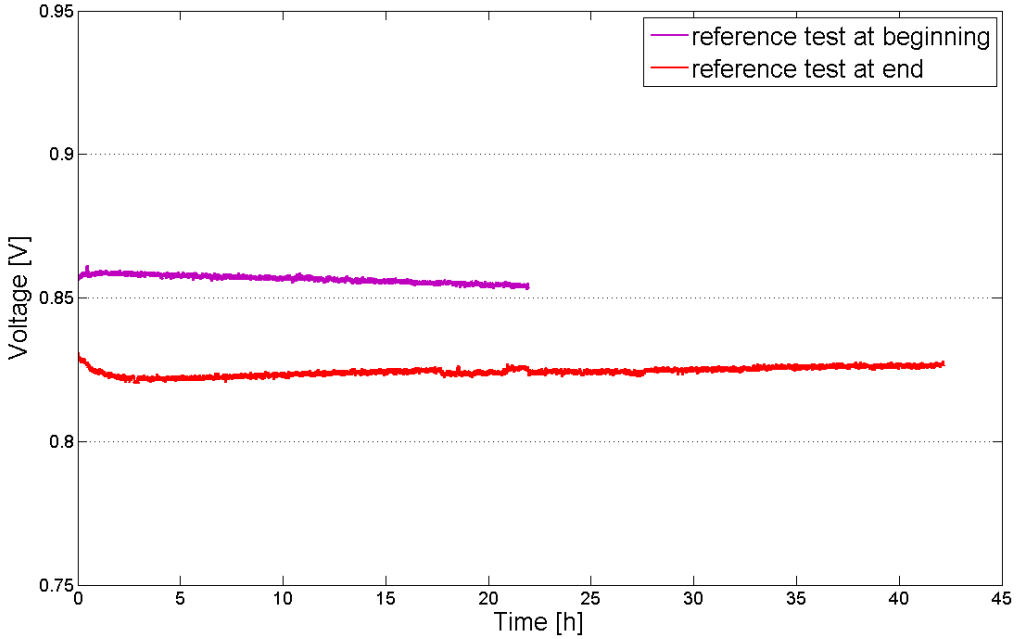

(a) Voltage over time

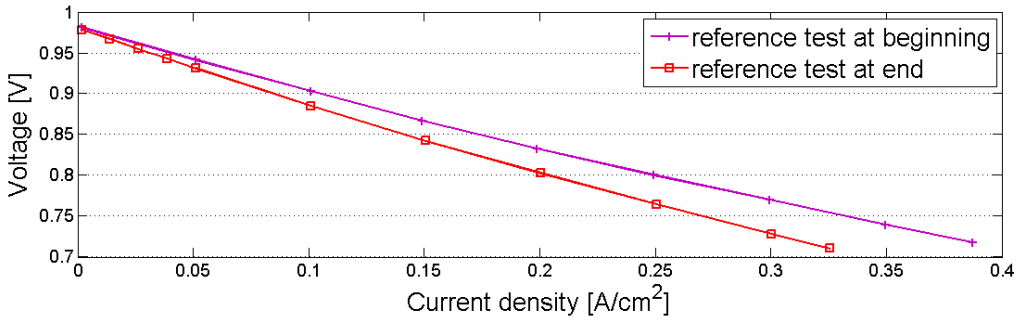

(b) I-V-curves, measured at the end of each test

Figure 6.1: Reference tests

$c(H_2)$	$c(H_2O)$	$c(CO)$	$c(CO_2)$
17.4 vol%	9.93 vol%	13.6 vol%	10.8 vol%
$c(H_2S)$	$c(SO_2)$	c(HC-mix)	$c(N_2)$
0.54 ppm	8.2×10^{-14}	227 ppm	48.4 vol%
$c(CH_4)$	$c(C_2H_4)$	$c(C_2H_6)$	$c(C_3H_6)$
227 ppm	1.3×10^{-10}	5.5×10^{-11}	3.3×10^{-16}

Table 6.1: Equilibrium concentrations of the test fuel gas at $T = 735\,°C$, $c(O_2(\text{anode})) = 3.91 \times 10^{-21}$); calculated for the standard fuel gas (see table 5.1) with the software *Gaseq* (see section 5.3)

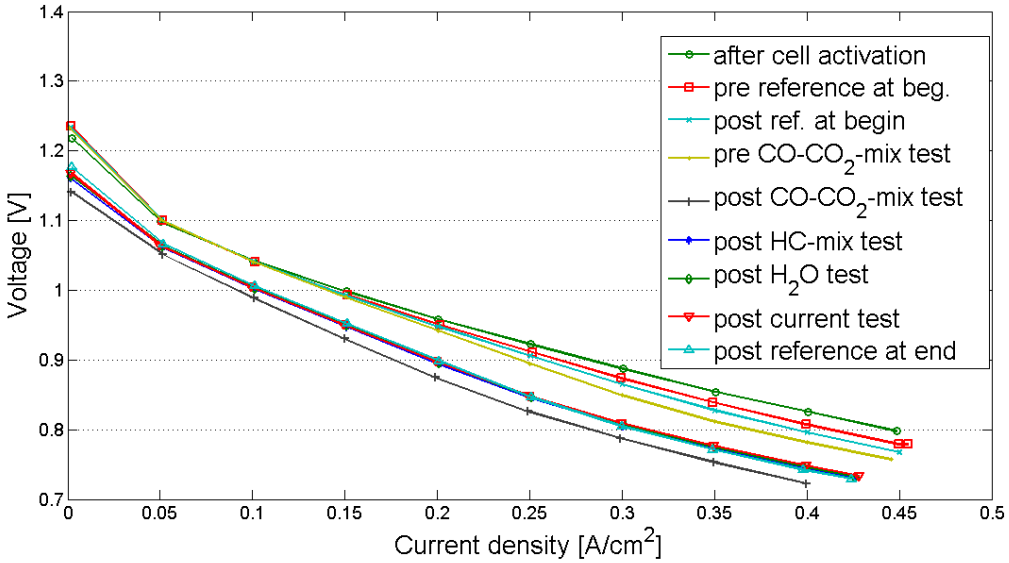

Figure 6.2: I-V-curves measured at the end of the regeneration periods, the H_2 flow was lowered from 17.74 Nl/h to 12 Nl/h after the first 4 curves (the upper 4 curves)

The calculated equilibrium concentrations of the standard fuel (as used in the reference tests) are given in table 6.1, they were computed using the software *Gaseq* (see end of section 5.3). The calculation of the expected voltage under equilibrium conditions using the Nernst equation gave results between 987.1 mV and 986.5 mV (deviation due to inexact equilibrium concentrations). The influence of the sulfur components on the Nernst-voltage can be neglected.

6.2 Carbon monoxide and carbon dioxide variation

In this test the concentrations of the CO-CO_2-mixture was varied against the H_2 concentration (see figure 6.3). Due to the failure of a mass flow controller the standard concentrations of the anode gases had to be changed for this test, so the voltage curve of this test cannot be compared to the reference tests.

The degradation after the preceding regeneration period took more than 11 h and was not fully finished before the end of the first test phase.

After changing the gas composition by lowering the H_2 and rising the CO-CO_2-mix amounts an expected drop in cell voltage occurs. In addition, the cell voltage decreases relatively steeply for about 2.3 h resp. 4.7 h before settling at a low degradation rate.

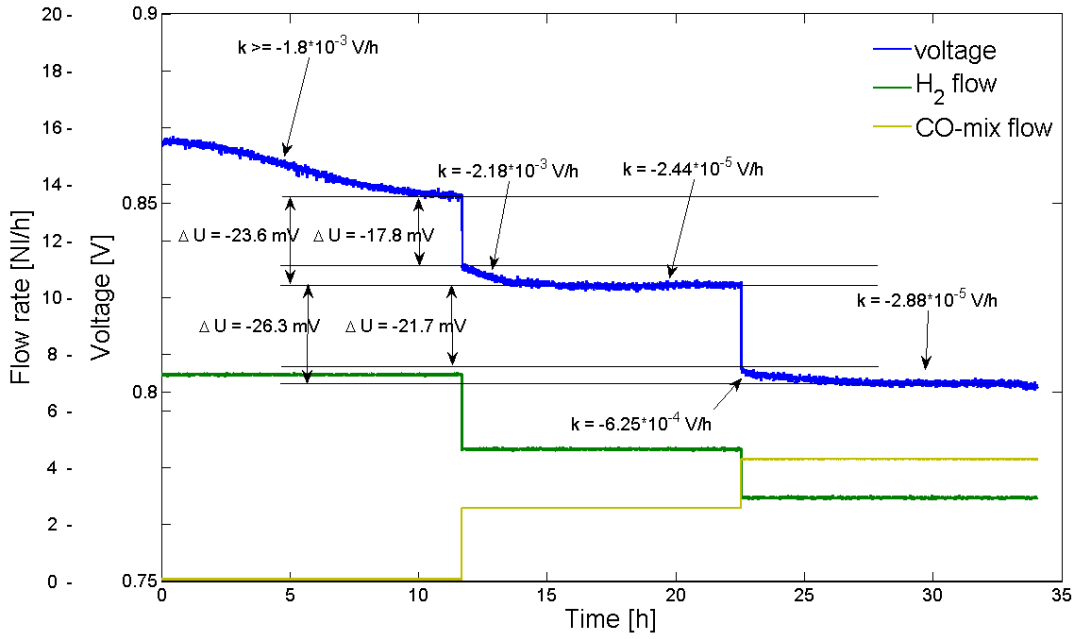

(a) Voltage over time

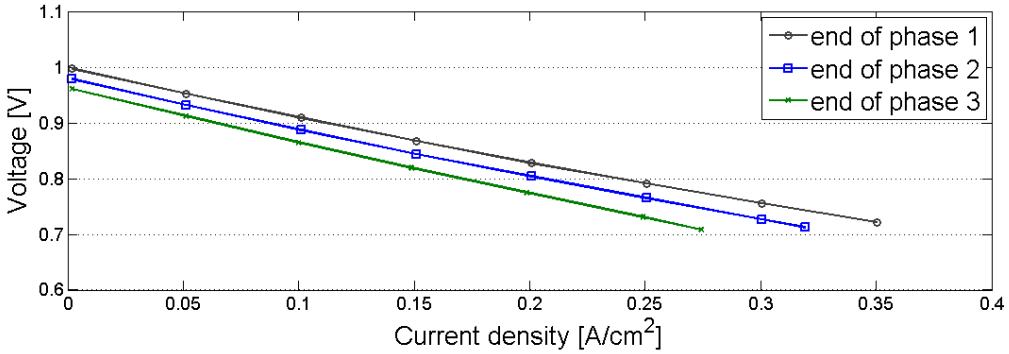

(b) I-V-curves measured at the end of each test phase

test phase	$c(H_2)$ [vol%]	$c(CO)$ [vol%]	$c(CO_2)$ [vol%]	η_{fu} [%]
1	42.3	0	0	15.47
2	27.3	8.49	6.07	18.12
3	17.3	14.2	10.1	20.46

(c) Varied test settings

Figure 6.3: CO and CO_2 variation test (constant settings differ from standard settings in other tests: $c(H_2O)$: 16.0 vol%, $c(H_2S)$: 0.25 ppm, $c(SO_2)$: 0.29 ppm, c(HC-mix): 738 ppm, $c(N_2)$: 42.8 vol%, I: 170 A/cm^2, T: 735 °C), η_{fu} (see equation 2.19) was calculated under the assumption of full hydrocarbon conversion

test phase	measured OCV [mV]	expected U_N [mV]
1	997.2	1003.6
2	978.6	984.6
3	960.3	976.2

Table 6.2: Open circuit voltages of the CO-CO_2 test; measured and calculated for chemical equilibrium using the Nernst equation

The slopes (k-values) of the fitting lines are quite uncertain due to jumps in voltage. The degradation directly after the voltage drops may be caused by both carbon deposition, due to a decreased S/C ratio and first order sulfur poisoning due to the lower H_2 concentration. The I-V-curves reflect the change in fuel utilisation. The measured OCVs and those calculcated for chemical equilibrium are shown in table 6.2.

Right after setting the anode flow for the test, the voltage over time graph shows a small positive slope for about 40 min. The reason of this behaviour is unknown.

6.3 Hydrocarbon variation

In this test the concentration of the hydrocarbon mix was varied (see figure 6.4). The small voltage steps to a lower level and back (e.g. in the second phase of figure 6.4(a)) are caused by an irregularity of the air mass flow at the anode side (see 5.1.2). In those regions the hydrogen amount was lowered to an unknown level and the water vapour amount was higher.

The first order degradation, caused by sulfur poisoning, in the first test phase had a negative slope of about 3.8 mV/h. It came to equilibrium after about 12 h.

At the concentration changes – the HC concentration was doubled at each step – increases of cell voltage of $\Delta U = 1.84\,\text{mV}$ or 0.23 % and $\Delta U = 3.21\,\text{mV}$ or 0.40 % were observed. Hence the hydrocarbons were either directly used or internally converted to hydrogen to a reasonable amount at these sulfur concentrations ($c(H_2S)$: 0.25 ppm, $c(SO_2)$: 0.29 ppm). Based on full hydrocarbon convertion the calculated H_2 amount increased for 0.63 % resp. 1.25 %. Unlike the CO-CO_2-mix test, there are no regions of steeper voltage change after the voltage steps. So the decrease in the S/C ratio seems to have no effect on carbon deposition. The relatively stable voltage curves have positive slopes. It may be the case that the increased amount of available H_2 is accounting for regeneration. The form of the I-V-curves at higher current values affirm that the additional hydrocarbons were converted.

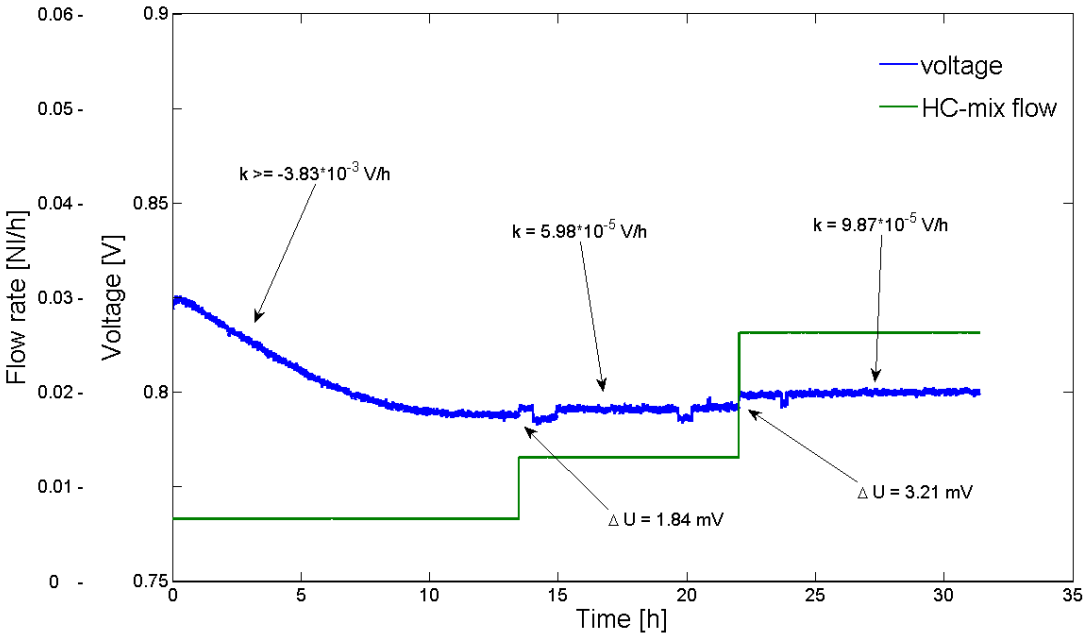

(a) Voltage over time

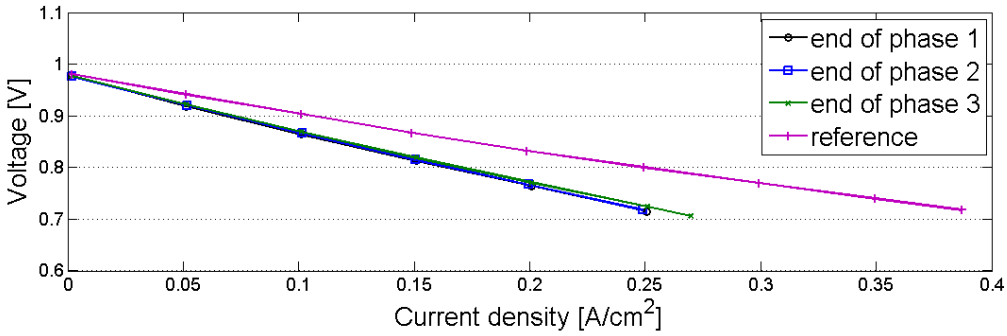

(b) I-V-curves measured at the end of each test phase

test phase	c(HC-mix) [ppm]
1	369
2	738
3	1476

(c) Varied test settings

Figure 6.4: Hydrocarbon variation test (constant settings: $c(H_2)$: 16.5 vol%, $c(H_2O)$: 10.7 vol%, $c(CO)$: 14.2 vol%, $c(CO_2)$: 10.1 vol%, $c(H_2S)$: 0.25 ppm, $c(SO_2)$: 0.29 ppm, $c(N_2)$: 48.4 vol%, I: 170 A/cm^2, T: 735 °C)

test phase	measured OCV [mV]	expected U_N [mV]
1	976.6	986.1
2	976.3	986,5
3	977.1	987.2

Table 6.3: Open circuit voltages of the HC test; measured and calculated for chemical equilibrium using the Nernst equation

The measured OCVs and those calculcated for chemical equilibrium are shown in table 6.3. Again, right after setting the flow rates for the first test phase, the voltage curve showed a positive slope.

6.4 Water vapour variation

In this test the concentration of the water vapour was varied against the nitrogen concentration (see figure 6.5). The jumps in the voltage graphs were again caused by irregularities of a mass flow controller.

In the first test phase the water content was decreased. The degradation due to sulfur poisoning after the regeneration period had a maximum slope in voltage decrease of 4.2 mV/h. This was the steepest voltage decrease due to sulfur poisoning observed in all tests. The duration of this degradation was similar to those in the other tests.

At the changeover to the next test phase the water content was raised to the standard value. A small negative voltage step of -0.78 mV occured. Then the voltage started to increase. The cell seems to regenerate from the first test phase, where besides sulfur poisoning also increased carbon deposition might have occured, because of the lowered water content. The second voltage step was 2.4 mV. The cell voltage was still increasing, but slower than in the previous test phase. The I-V-curves show, that the cell was operating at a higher power level with less water content in the fuel until a current density of about 130 A/cm^2.

The measured OCVs and those calculcated for chemical equilibrium are shown in table 6.4. Once more, right after the start of the test, the voltage curve showed a positive slope.

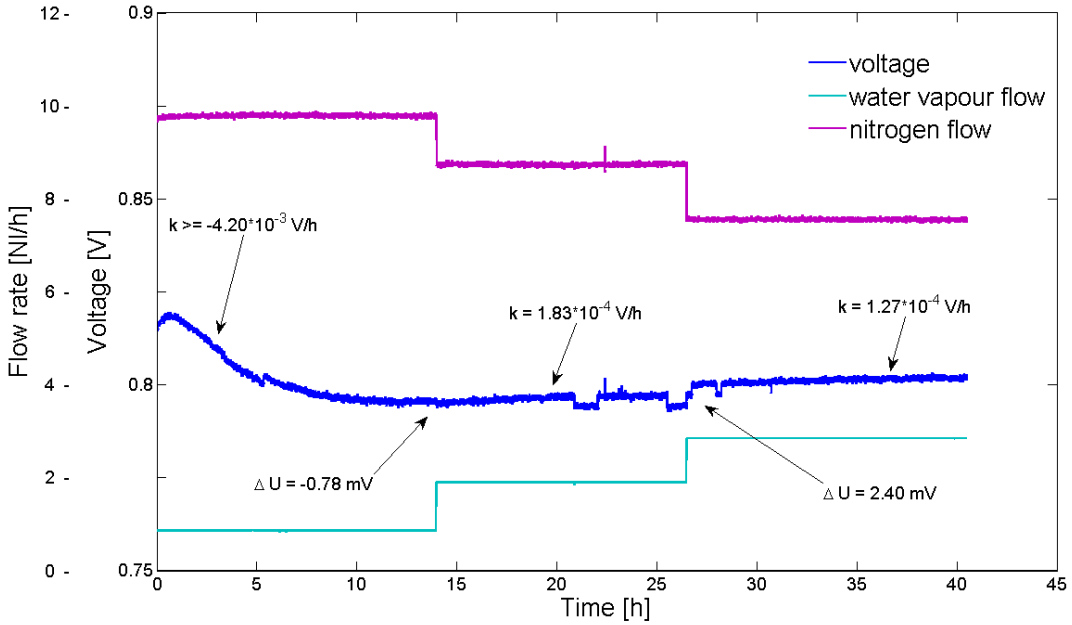

(a) Voltage over time

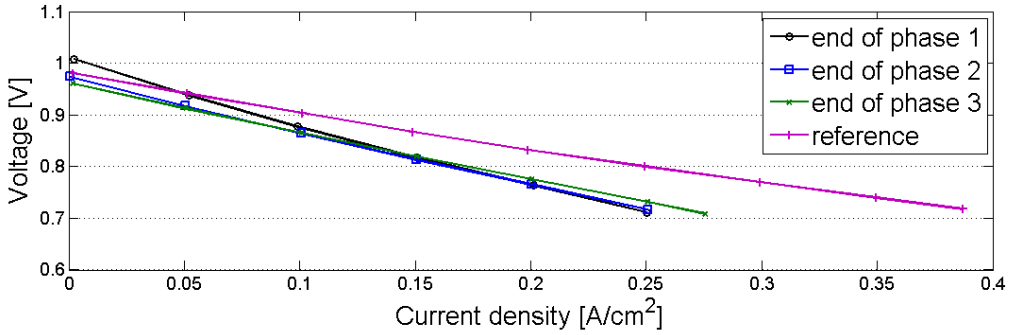

(b) I-V-curves measured at the end of each test phase

test phase	$c(H_2O)$ [vol%]	$c(N_2)$ [vol%]
1	4.85	54.3
2	10.7	48.4
3	16.0	43.1

(c) Varied test settings

Figure 6.5: Water steam variation test ($c(H_2)$: 16.5 vol%, $c(CO)$: 14.2 vol%, $c(CO_2)$: 10.1 vol%, $c(H_2S)$: 0.25 ppm, $c(SO_2)$: 0.29 ppm, c(HC-mix): 738 ppm, I: 170 A/cm^2, T: 735 °C)

6.5 Current variation

In this test the effect of the current drawn on sulfur poisoning was investigated. The standard gas mixture is led to the anode, while in the first phase no current is drawn and at the beginning of the second and third phase the current is raised. The graphs of this test are shown in figure 6.6. The current ripples, that can be seen in the graph, were caused by the electronic load (see also section 5.1.2) and did not seem to have any impact on the measurement.

The first order degradation after the regeneration period was very fast. It came to a slower degradation already after about 2.5 h. The degradation rate of the cell at the end of the first test phase was relatively high. It became less steep at the change to the next phase. The degradation rate decreased further to the value of 0.015 mV/h in the last test phase.

The degradation of the cell over the test period was very small. So no difference can be seen in the I-V-curves.

6.6 Temperature variation

In this test the cell temperature was varied from the standard parameters (see figure 6.7). The temperature was raised to 785 °C and became stable before the test started, but during the test the furnace did not keep the temperature stable. The oven temperature and the cell temperature were both monitored and had the same changing values. Due to this problem no reasonable values of the slopes of the voltage curve could be measured. The reason for the abnormal voltage curve in phase 3 can probably be explained by the mass flow controller problems.

The temperature dropped by 4 degrees in the first test phase, increased by 2.4 degrees in the second phase and dropped again by 5.5 degrees during the third phase. The change in temperature at the changeover to the second phase caused a relatively small voltage

test phase	measured OCV [mV]	expected U_N [mV]
1	1008.3	1001.7
2	973.7	986.5
3	960.5	975.8

Table 6.4: Open circuit voltages of the water vapour test; measured and calculated for chemical equilibrium using the Nernst equation

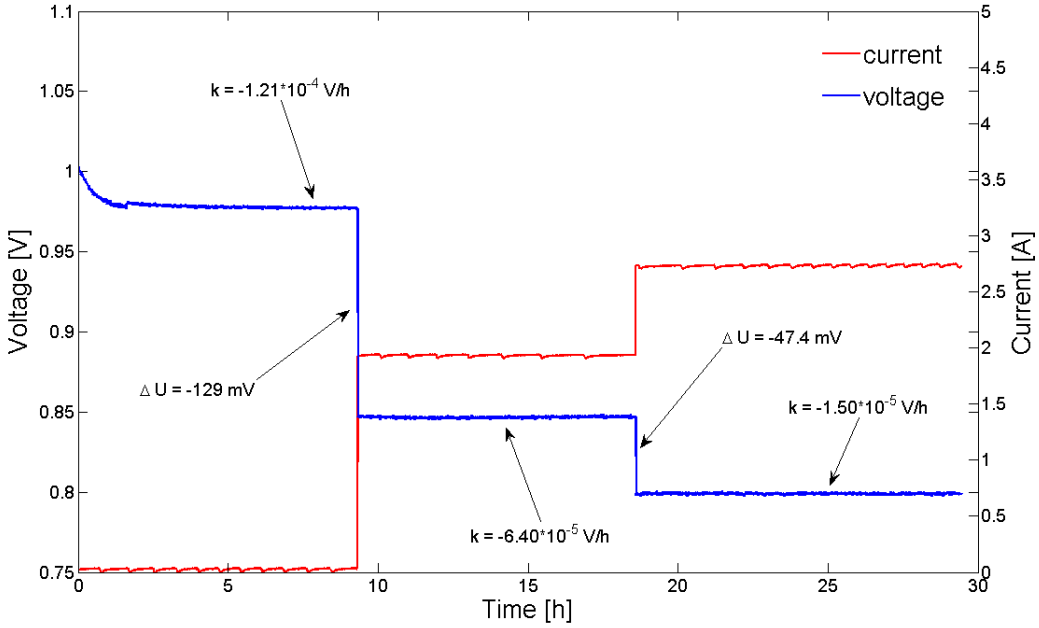

(a) Voltage over time

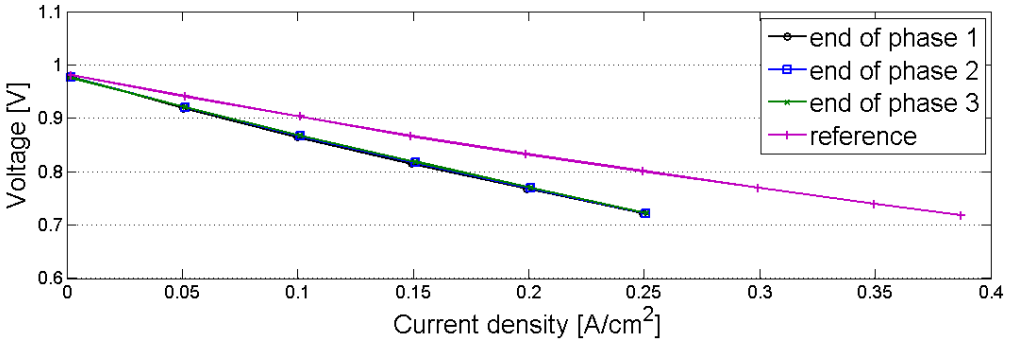

(b) I-V-curves measured at the end of each test phase

test phase	I [mA/cm^2]	I [A/cell]
1	0	0
2	120	1.92
3	170	2.72

(c) Varied test settings

Figure 6.6: Current variation test ($c(H_2)$: 16.5 vol%, $c(H_2O)$: 10.7 vol%, c(CO): 14.2 vol%, $c(CO_2)$: 10.1 vol%, $c(H_2S)$: 0.25 ppm, $c(SO_2)$: 0.29 ppm, c(HC-mix): 738 ppm, $c(N_2)$: 48.4 vol%, T: 735 °C)

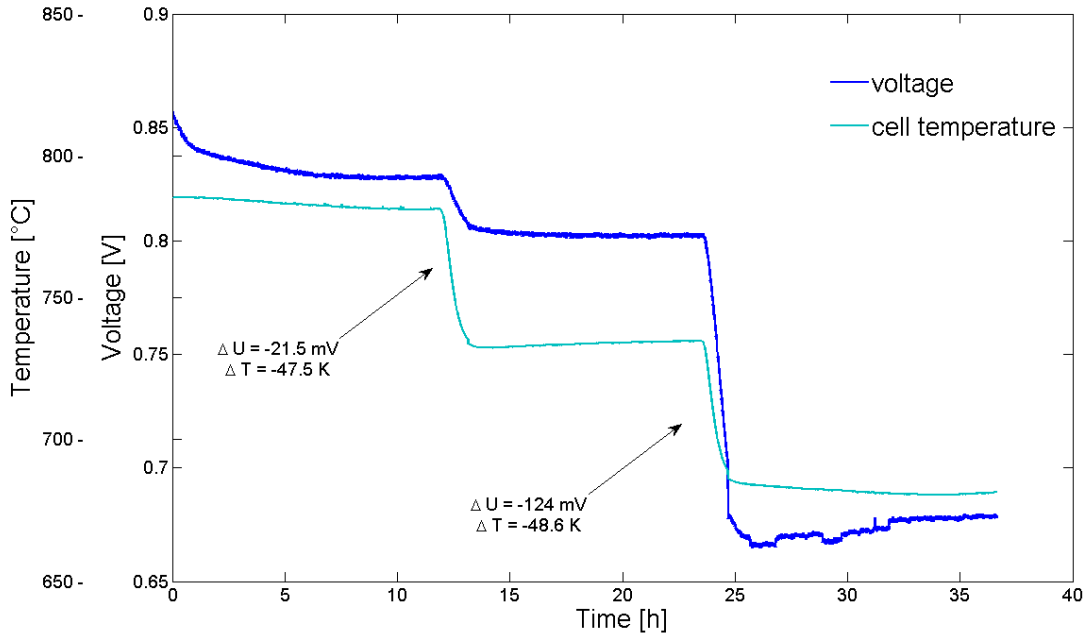

(a) Voltage over time

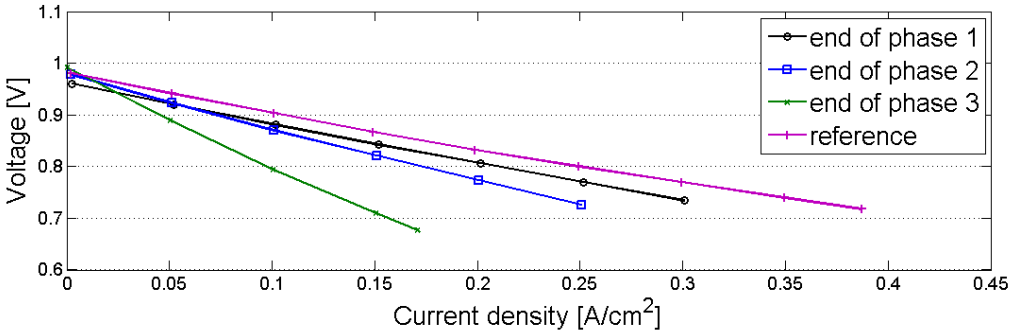

(b) I-V-curves measured at the end of each test phase

test phase	T[°C]
1	785 to 781
2	732.3 to 734.7
3	686 to 680.5

(c) Varied test settings

Figure 6.7: Temperature variation test ($c(H_2)$: 16.5 vol%, $c(H_2O)$: 10.7 vol%, c(CO): 14.2 vol%, $c(CO_2)$: 10.1 vol%, $c(H_2S)$: 0.25 ppm, $c(SO_2)$: 0.29 ppm, c(HC-mix): 738 ppm, $c(N_2)$: 48.4 vol%, I: 170 A/cm^2)

test phase	T_m [°C] at measurement	measured OCV [mV]	expected U_N [mV] at T_m
1	781	960.5	969.0
2	734.7	977.7	986.6
3	681.2	991.9	1006.5

Table 6.5: Open circuit voltages of the water vapour test; measured and calculated for chemical equilibrium using the Nernst equation

drop ($\Delta_T = 47.5\,\mathrm{K}$ and $\Delta_U = -21.5\,\mathrm{mV}$). At the second step a higher drop occured ($\Delta_T = -48.6\,\mathrm{K}$ and $\Delta_U = -124\,\mathrm{mV}$). This behaviour was expected as the temperature of 685 °C is quite low for SOFC operation.

The OCVs were rising as expected with the lower temperature. The measured OCVs and those calculcated for chemical equilibrium are shown in table 6.5.

6.7 Table of characteristic numbers of all tests

For comparison, a summary of measured characteristic numbers is given in table 6.6.

test	first slope	$\Delta_{\text{ref},1}U$	phase 1		$\Delta_{1,2}U$	phase 2		$\Delta_{2,3}U$	phase 3	
			k_1	k_2		k_1	k_2		k_1	k_2
(2) H_2S-test[1]	—	—	> -2.2		< -19.5[2]	-0.32		-7.7	-1.5	-0.088
(3) SO_2-test[1]	—	—	-0.72		-25[2]	~ -2.2		-3.6	-1.5	0.071
(4) CO-CO_2-test [3]	pos.	11.8	> -1.8		-23.6	-2.2	-0.025	-26.3	-0.63	-0.029
(5) HC-Test	pos.	-45.9	> -3.8		1.84	—	0.060	3.21	—	0.099
(6) H_2O-test	pos.	-44.4	> -4.2		-0.78	—	0.18	2.4	—	0.13
(7) current-test	—	136.9	—	-0.12	-129	—	-0.064	-47.4	—	-0.015
(8) temperature-test	—	-12.4	—	—	-21.5	—	—	-124	—	—

[1] tested by Rittenschober [54]
[2] value is $\Delta_{\text{ref},2}U$
[3] standard parameters were changed in this test

Table 6.6: Units: [U] = mV, [slopes k_i] = mV/h; reference voltage $U_{\text{ref}} = 840\,\text{mV}$

7 Conclusion and outlook

The degradation of solid oxide fuel cells due to sulfur compounds in the fuel gas was investigated. Characteristic durations and rates of degradation could be measured in the conducted tests.

The cell voltage did not come back to the initial level when the sulfur compounds were removed from the fuel stream and regeneration periods with pure hydrogen were conducted. The observed first order degradation took a time of at least 10 hours at 735 °C, when current was drawn from the cell. This was clearly less time than when the cell had the very first contact to any sulfur compounds (reported in [54]). So sulfur adsorption was not fully reversible in the experiments done. Maybe much longer periods of operation with pure hydrogen would have slightly improved the regeneration from sulfur poisoning, but would have most likely not revealed to full reversibility.

These periods of first order degradation had a longer duration than reported in [63] at comparable testing conditions with thinner anodes. This goes along with the assumption made in [60], predicting longer degradation periods for cells of the ASC type.

When using the standard fuel and its variations the I-V-curves show no big change in slope at low currents throughout all tests. This goes along with the assumption of low activation polarization for SOFC anodes [18].

When varying the amount of hydrocarbons in the fuel, it could be revealed that hydrocarbons were converted in the SOFC anode under the influence of sulfur poisoning. An increase in cell voltage occured when supplying additional hydrocarbons to the cell at the total sulfur concentration of 0.54 ppm. This confirms the results of investigations of methane conversion attained in open circuit measurements described in [45].

Rittenschober, who varied H_2S and SO_2 concentrations, arrived at the conclusion that the total sulfur content in the fuel is crucial for the sulfur poisoning effect on the tested SOFC [54].

In another test the CO and CO_2 amounts in the fuel were increased, while the hydrogen amount was decreased and the concentrations of sulfur compounds remained the same. This did not only lead to an immediate voltage drop, but also to gradual degradation

during the first hours after the increase.

The observed degradation rate decreased to some extend in the test, while the electrical current was increased. Improvements of the cell operation due to higher currents as reported by some groups can neither be confirmed nor rebutted. Longer testing periods or the introduction and removal of sulfur compounds at different current settings would be necessary to evaluate this effect.

The temperature variation test revealed a big difference in power output drop when changing from 785 to 735 and further to 685 °C. The observed voltage drop at the second temperature step was 5 times as big as at the first step. Degradation rates at different temperature levels can not be compared because of temperature stability issues.

The design of the test setup worked well. Particularly the achieved gas tightness was satisfactory. Some technical problems had influence on the experiments. Those have to be solved for future measurements. Furthermore, additional methods for output gas analysis and electrical impedance spectroscopy are suggested.

In order to further use the obtained results, the same test matrix without any sulfur compounds should be conducted. Then the influence of sulfur could be stated and quantified more precisely. In some test phases it will be necessary to allow more time for the measurements.

References

[1] M.M. Mench. *Fuel cell engines*, chapter 3. John Wiley & Sons, 2008.

[2] P.J. Linstrom and W.G. Mallard. Eds., NIST Chemistry WebBook. NIST Standard Reference database number 69, June 2005. national Institute of Standards and Technology, Gaithersburg MD, 20899 (http://webbook.nist.gov).

[3] Johnson Matthey PLC as Fuel Cell Today. The fuel cell today industry review 2011, Sep 14, 2011. http://www.fuelcelltoday.com/analysis/industry-review/2011/the-industry-review-2011 accessed on May 25, 2012.

[4] D. Carter and J. Wing. Fuel cells from demonstration to mass production, Apr 25, 2012. http://www.fuelcelltoday.com/analysis/analyst-views/2012/12-04-25-fuel-cells-from-demonstration-to-mass-production accessed on May 25, 2012.

[5] R. Steinberger-Wilckens. European SOFC technology status and trends. *ECS Transactions*, 35(1):19–29, 2011.

[6] B.E. Logan. *Microbial Fuel Cells*, chapter 1. Wiley-Interscience, 2008.

[7] AS Elcogen. SOFC single cell description. http://www.elcogen.com/index.php/description accessed on Sep 7, 2012.

[8] S.C. Singhal and K. Kendall. Introductions to SOFCs. In *High Temperature Solid Oxide Fuel Cells*, Electronics & Electrical, chapter 1. Elsevier, 2003.

[9] K. Sasaki, K. Haga, T. Yoshizumi, D. Minematsu, E. Yuki, R. Liu, C. Uryu, T. Oshima, T. Ogura, Y. Shiratori, K. Ito, M. Koyama, and K. Yokomoto. Chemical durability of solid oxide fuel cells: Influence of impurities on long-term performance. *Journal of Power Sources*, 196(22):9130 – 9140, 2011.

[10] J. Bao, G. N. Krishnan, P. Jayaweera, J. Perez-Mariano, and A. Sanjurjo. Effect of various coal contaminants on the performance of solid oxide fuel cells: Part I. accelerated testing. *Journal of Power Sources*, 193(2):607 – 616, 2009.

[11] J. Bao, G. N. Krishnan, P. Jayaweera, K.H. Lau, and A. Sanjurjo. Effect of various coal contaminants on the performance of solid oxide fuel cells: Part II. ppm and sub-ppm level testing. *Journal of Power Sources*, 193(2):617 – 624, 2009.

[12] J. Bao, G. N. Krishnan, P. Jayaweera, and A. Sanjurjo. Effect of various coal gas contaminants on the performance of solid oxide fuel cells: Part III. synergistic effects. *Journal of Power Sources*, 195(5):1316 – 1324, 2010.

[13] F .N. Cayan, M. Zhi, S. R. Pakalapati, I. Celik, N. Wu, and R. Gemmen. Effects of coal syngas impurities on anodes of solid oxide fuel cells. *Journal of Power Sources*, 185(2):595 – 602, 2008.

[14] V. Alzate-Restrepo and J. M. Hill. Carbon deposition on Ni/YSZ anodes exposed to CO/H2 feeds. *Journal of Power Sources*, 195(5):1344 – 1351, 2010.

[15] J. Bogild Hansen and J. Rostrup-Nielsen. Sulfur poisoning on Ni catalyst and anodes. In W. Vielstich, H. Yokokawa, and H.A. Gasteiger, editors, *Handbook of fuel cells*, volume 6: Adcances in electrocatalysis, materials, diagnostics and durability, part 5, chapter 65. Wiley, 2009.

[16] B. Zhu. Proton and oxygen ion-mixed-conducting ceramic composites and fuel cells. *Solid State Ionics*, 145:371 – 380, 2001.

[17] S. B. Adler and W. G. Bessler. Elementary kinetic modeling of solid oxide fuel cell electrode reactions. In W. Vielstich, H. Yokokawa, and H.A. Gasteiger, editors, *Handbook of fuel cells*, volume 5: Adcances in electrocatalysis, materials, diagnostics and durability, part 3, chapter 29. Wiley, 2009.

[18] N. Frank. *Umsetzung von Kohlenwasserstoffen in SOFCs*. PhD thesis, TU Munich, 2009.

[19] M.M. Mench. *Fuel cell engines*, chapter 4. John Wiley & Sons, 2008.

[20] J.H. Hirschenhofer, Parsons Corporation, and Federal Energy Technology Center (U.S.). *Fuel cell handbook*, chapter 3. U.S. Dept. of Energy, Office of Fossil Energy, Federal Energy Technology Center, 4 edition, 1998.

[21] M. Bieber. *Messmethoden zur Untersuchung der Kohlenstoffablagerung an nickelhaltigen SOFC-Anoden beim Betrieb mit Methan*. PhD thesis, Technische Universität München, 2010.

[22] S. Mekhilef, R. Saidur, and A. Safari. Comparative study of different fuel cell technologies. *Renewable and Sustainable Energy Reviews*, 16(1):981 – 989, 2012.

[23] F. Barbir. *Pem Fuel Cells: Theory And Practice*, chapter 4. Academic Press Sustainable World Series. Elsevier Academic Press, 2005.

[24] A. Heinzel, M. Cappadonia, U. Stimming, K. V. Kordesch, and J. C. T. de Oliveira. Fuel cells. In *Ullmann's Encyclopedia of Industrial Chemistry*. Wiley-VCH Verlag GmbH & Co. KGaA, 2000.

[25] B. Sorensen. *Hydrogen and fuel cells: Emerging technologies and applications*, chapter 3. Sustainable world series. Elsevier Academic Press, 2005.

[26] Gunther Weirum. Personal communication. Graz, Sept. 27, 2012.

[27] K.A. Adamson. *Stationary Fuel Cells: An Overview*, chapter 2.4. Elsevier Science, 2007.

[28] A. Kirubakaran, S. Jain, and R.K. Nema. A review on fuel cell technologies and power electronic interface. *Renewable and Sustainable Energy Reviews*, 13(9):2430 – 2440, 2009.

[29] M. Yashima, M. Kakihana, and M. Yoshimura. Metastable-stable phase diagrams in the zirconia-containing systems utilized in solid-oxide fuel cell application. *Solid State Ionics*, 86-88, Part 2(0):1131 – 1149, 1996.

[30] J. Larminie and A. Dicks. *Fuel cell systems explained*, page 15. J. Wiley, 2003.

[31] P. Gouerec, L. Poletto, J. Denizot, E. Sanchez-Cortezon, and J.H. Miners. The evolution of the performance of alkaline fuel cells with circulating electrolyte. *Journal of Power Sources*, 129(2):193 – 204, 2004.

[32] M. Cifrain and K. Kordesch. Hydrogen/oxygen (air) fuel cells with alkaline electrolytes. In W. Vielstich, A. Lamm, and H.A. Gasteiger, editors, *Handbook of fuel cells*, volume 1, part 4, chapter 14. Wiley, 2003.

[33] N. Q. Minh K. Kendall and S. C. Singhal. Cell and stack designs. In *High Temperature Solid Oxide Fuel Cells*, Electronics & Electrical, chapter 8. Elsevier, 2003.

[34] M.M. Mench. *Fuel cell engines*, chapter 7. John Wiley & Sons, 2008.

[35] M.C Williams, J.P Strakey, and Subhash C Singhal. U.S. distributed generation fuel cell program. *Journal of Power Sources*, 131(12):79 – 85, 2004.

[36] N. M. Sammes T. Ishihara and O. Yamamoto. Electrolytes. In *High Temperature Solid Oxide Fuel Cells*, Electronics & Electrical, chapter 4. Elsevier, 2003.

[37] T. Kawada and J. Mizusaki. Current electrolytes and catalysts. In W. Vielstich, H. Yokokawa, and H.A. Gasteiger, editors, *Handbook of fuel cells*, volume 4: Fuel Cell Technology and Applications, part 8, chapter 70. Wiley, 2009.

[38] H. Salmang and H. Scholze. Strukturen. In R. Telle, editor, *Keramik*, pages 9–174. Springer Berlin Heidelberg, 2007.

[39] J.F. Baumard and P. Abelard. Defect structure and transport properties of ZrO2-based solid electrolytes. *Advances in Ceramics*, 12:555–571, 1984.

[40] R.J. Stafford, S.J. Rothman, and J.L. Routbort. Effect of dopant size on the ionic conductivity of cubic stabilised ZrO2. *Solid State Ionics*, 37(1):67 – 72, 1989.

[41] M.F. Trubelja and V.S. Stubican. Ionic conductivity in the hafnia-R2O3 systems. *Solid State Ionics*, 49(0):89 – 97, 1991.

[42] A. McEvoy. Anodes. In *High Temperature Solid Oxide Fuel Cells*, Electronics & Electrical, chapter 6. Elsevier, 2003.

[43] J. A. Kilner and J. T. S. Irvine. New oxide cathodes and anodes. In W. Vielstich, H. Yokokawa, and H.A. Gasteiger, editors, *Handbook of fuel cells*, volume 5: Adcances in electrocatalysis, materials, diagnostics and durability, part 3, chapter 32. Wiley, 2009.

[44] K. Sasaki, K. Susuki, A. Iyoshi, M. Uchimura, N. Imamura, H. Kusaba, Y. Teraoka, H. Fuchino, K. Tsujimoto, Y. Uchida, and N. Jingo. H2S poisoning of solid oxide fuel cells. *Journal of The Electrochemical Society*, 153(11):A2023–A2029, 2006.

[45] A. Hagen, J. F.B. Rasmussen, and K. Thydén. Durability of solid oxide fuel cells using sulfur containing fuels. *Journal of Power Sources*, 196(17):7271 – 7276, 2011.

[46] A. Weber. *Entwicklung von Kathodenstrukturen für die Hochtemperatur-Brennstoffzelle SOFC*. PhD thesis, Universität Fridericiana Karlsruhe, 2002.

[47] C Sun, R. Hui, and J. Roller. Cathode materials for solid oxide fuel cells: a review. *J Solid State Electrochem*, 14:11251144, 2010.

[48] R. Merkle, J. Maier, and J. Fleig. Mechanistic understanding and electrochemical modeling of mixed conducting (SOFC) electrodes. In W. Vielstich, H. Yokokawa, and H.A. Gasteiger, editors, *Handbook of fuel cells*, volume 5: Adcances in electrocatalysis, materials, diagnostics and durability, part 3, chapter 28. Wiley, 2009.

[49] J. N. Kuhn, N. Lakshminarayanan, and U. S. Ozkan. Effect of hydrogen sulfide on the catalytic activity of Ni-YSZ cermets. *Journal of Molecular Catalysis A: Chemical*, 282(12):9 – 21, 2008.

[50] M.M. Mench. *Fuel cell engines*. John Wiley & Sons, 2008.

[51] H. Miao, W. G. Wang, T. S. Li, T. Chen, S. S. Sun, and C. Xu. Effects of coal syngas major compositions on Ni/YSZ anode-supported solid oxide fuel cells. *Journal of Power Sources*, 195(8):2230 – 2235, 2010.

[52] L. Gaines and T. Levinson. Idling - cruising the fuel in-efficiency expressway. Technical report, Center for Transportation Research, Energy Systems Division, Argonne National Laboratory, September 2009, Updated June 2011. ANL-11/08.

[53] J. Rechberger, M. Reissig, M. Hauth, and P. Prenninger. SOFC system development at AVL. Lucerne, Switzerland, 2012. 10th European SOFC Forum. A0401.

[54] M. Rittenschober. Working title: Schwefelverträglichkeit von SOFCs. Master's thesis, Graz University of Technology, 2012. work on thesis in progress.

[55] ASTM. Standard, 2011. ASTM D975.

[56] European Union. Norm, 2010. EN 590:2010.

[57] P. Lohsoontorn, D.J.L. Brett, and N.P. Brandon. Thermodynamic predictions of the impact of fuel composition on the propensity of sulphur to interact with Ni and ceria-based anodes for solid oxide fuel cells. *Journal of Power Sources*, 175(1):60 – 67, 2008.

[58] M. Mogensen and P. V. Hendriksen. Testing of electrodes, cells and short stacks. In Subhash C Singhal and Kevin Kendal, editors, *High Temperature Solid Oxide Fuel Cells*, chapter 10, pages 261 – 289. Elsevier Science, Amsterdam, 2003.

[59] J.R. Rostrup-Nielsen, J.B. Hansen, S. Helveg, N. Christiansen, and A.-K. Jannasch. Sites for catalysis and electrochemistry in solid oxide fuel cell (SOFC) anode. *Applied Physics A: Materials Science and Processing*, 85(4):427–430, 2006.

[60] L. Yang, Z. Cheng, M. Liu, and L. Wilson. New insights into sulfur poisoning behavior of Ni-YSZ anode from long- term operation of anode-supported SOFCs. *Energy and Environmental Science*, 3:1804–1809, 2010.

[61] S. Zha, Z. Cheng, and M. Liu. Sulfur poisoning and regeneration of Ni-based anodes in solid oxide fuel cells. *Journal of The Electrochemical Society*, 154(2):B201–B206, 2007.

[62] A. Lussier, S. Sofie, J. Dvorak, and Y.U. Idzerda. Mechanism for SOFC anode degradation from hydrogen sulfide exposure. *International Journal of Hydrogen Energy*, 33(14):3945 – 3951, 2008.

[63] Y. Matsuzaki and I. Yasuda. The poisoning effect of sulfur-containing impurity gas on a SOFC anode: Part I. Dependence on temperature, time, and impurity concentration. *Solid State Ionics*, 132:261 – 269, 2000.

[64] D. Mogensen, J.-D. Grunwaldt, P.V. Hendriksen, K. Dam-Johansen, and J.U. Nielsen. Internal steam reforming in solid oxide fuel cells: Status and opportunities of kinetic studies and their impact on modelling. *Journal of Power Sources*, 196(1):25 – 38, 2011.

[65] J. F.B. Rasmussen and A. Hagen. The effect of H2S on the performance of Ni–YSZ anodes in solid oxide fuel cells. *Journal of Power Sources*, 191(2):534 – 541, 2009.

[66] F. B. Wede. Working title: Konzept für eine 10 kW SOEC Elektrolyse Anlage. Master's thesis, Graz University of Technology, 2012. work on thesis in progress.

[67] A. Hagen. Personal communication. Email, Apr. 19, 2012.